Review of Fluid Slip over Superhydrophobic Surfaces and Its Dependence on the Contact Angle

ARTICLE *in* INDUSTRIAL & ENGINEERING CHEMISTRY RESEARCH · MARCH 2008

Impact Factor: 2.59 · DOI: 10.1021/ie0712941

2 AUTHORS:

Roman Voronov
New Jersey Institute of Technology
33 PUBLICATIONS **363** CITATIONS

SEE PROFILE

Dimitrios Papavassiliou
University of Oklahoma
175 PUBLICATIONS **1,538** CITATIONS

SEE PROFILE

100TH ANNIVERSARY REVIEW

Review of Fluid Slip over Superhydrophobic Surfaces and Its Dependence on the Contact Angle

Roman S. Voronov and Dimitrios V. Papavassiliou

School of Chemical, Biological and Materials Engineering, University of Oklahoma, Norman, Oklahoma 73019-1004

Lloyd L. Lee*

Chemical and Materials Engineering, California State University, Pomona, California 91768

A review of the characteristics of hydrophobicity is presented, with the goal of investigating the relationship, if any, between the contact angle (a macroscopically observed property) and the slip length (a microscopic phenomenon). An analysis of simulations, and of their evolution through the years, sheds light on some inherent differences between contact angle and slip length behavior on flat and patterned surfaces. Previous studies lead to the conclusion that epitaxial layering of fluid near the solid is intricately related to the magnitude of fluid slip. Epitaxial layer data help to explain unexpected slip length behavior in relation to the contact angle, and reported inconsistencies between slip length experiments and simulations. Therefore, it seems that solids that can produce favorable epitaxial layering of the fluid will cause larger slip. Dimensional analysis is used to elucidate the contact angle−slip length relationship. Results can be applied to the development of artificial supersolvophobic surfaces that would exhibit predictable fluid slip with important practical applications.

I. Introduction

Interest in superhydrophobic surfaces has been growing in the past decade, because of their potential applications in friction−drag reduction, anticorrosive protective coatings, microfluidics (microchannels and reactors, lab-on-a-chip devices),[1,2] and self-cleaning surfaces, such as window glasses, paints, and fabrics. It is commonly believed that a water (or fluid)-repellant surface, such as a hydrophobic (or solvophobic) surface, can result in friction−drag reduction.[3−6] The reason is the generation of fluid slip at the solid/fluid interface—a microscopic phenomenon that has recently caused a renewed interest into the applicability of the well-established no-slip boundary condition to the Navier−Stokes equations. As common sense would dictate, the more a fluid slips past a surface, the less friction drag there is. Significant drag reduction in fluid flow would have enormous economic and technological impact in microfluidics and in biomedical devices.[4] In fact, artificial design of superhydrophobic surfaces is a very active area of research today[7] (although the quest for friction reduction via water-repellant surface treatment started long ago).[8]

When a superhydrophobic surface is being designed in a laboratory, it is typically difficult to experimentally measure how easily water will slip past the surface, or the amount of friction−drag reduction that will occur, because of the high cost of the experimental apparatus, the small size of the available sample, and the microscopic nature of the slip phenomenon. Despite the multitude of experimental evidence (see section III) and a plethora of theoretical models for the mechanism of slip (see section IV.c), there is currently no universally accepted, complete analytical method that can predict the occurrence of interfacial slip, or its magnitude, at solid−liquid boundaries (although if the slip length is known, there exist theories and numerical codes that allow the prediction of drag reduction for laminar[4] and turbulent[3,6] flows). A more mundane approach to testing the surface is to measure the contact angle of water on the surface being designed (see section I.b)—this is a macroscopic measure of hydrophobicity, which measures the static repulsion between the surface and water—and hope that designing a surface in such a way that the contact angle is maximized will result in minimum friction drag. Intuitively, this approach seems to be correct. The two characteristics of hydrophobicity (slip length and contact angle) should be directly related to each other; however, in practice, this hypothesis has been neither verified nor disproved. A review of contact angle and slip length simulation results is provided herein (see sections II and III.b), to elucidate the nature of such relationship (see section IV). Such knowledge would be beneficial to superhydrophobic surface design. If, indeed, this relationship exists, does it always hold or do new, better tools need to be developed to predict what makes a good friction−drag reducer and what does not? These are some of the questions that we attempt to answer.

Abundant contact angle data exist in the literature, in contrast to slip length measurements (of which there are not as many). The main difficulty with measuring slip lengths is that the measurements must be accurate in the microscale, on the order

* To whom correspondence should be addressed. Tel.: (909) 869-2423. Fax: (909) 869-6920.

10.1021/ie0712941 CCC: $40.75
Published on Web 03/25/2008

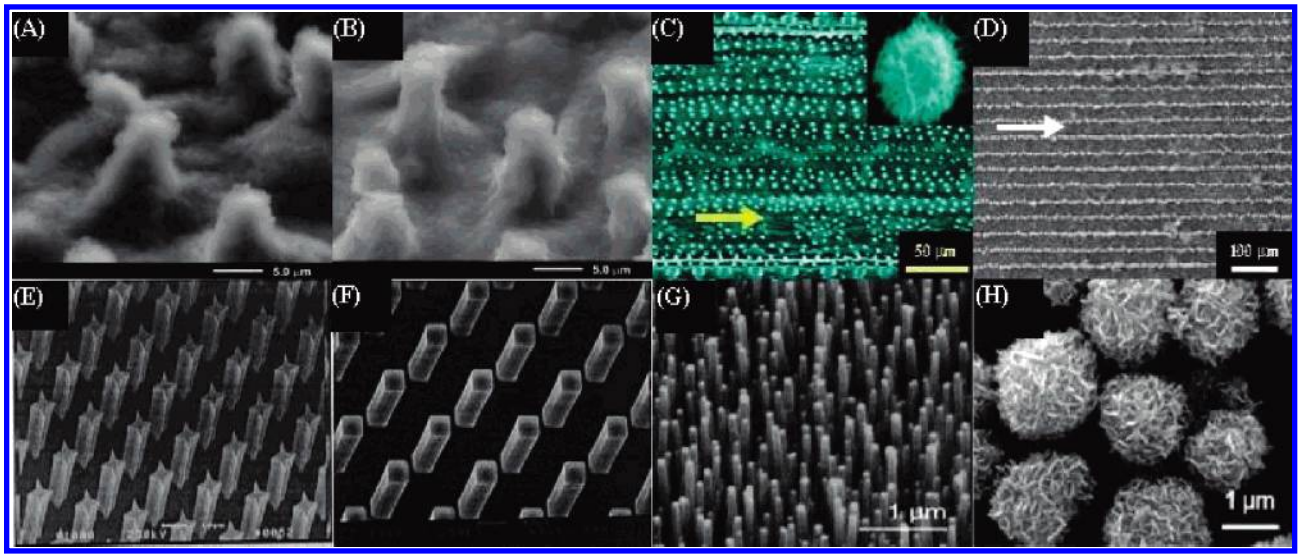

Figure 1. (A and B) High-magnification SEM images of (A) the natural lotus leaf and (B) its positive replica; they almost have the same surface morphology on both the microscale and the nanoscale. (Bar = 5 μm. Reprinted with permission from Sun et al.[20] Copyright 2005, American Chemical Society.) (C and D) Large-scale SEM image of the surface of a rice leaf (*Oryza sativa*) (C) with different magnifications (bar = 50 μm) and (D) the top view of a rice-like ACNT film (bar = 100 μm). (Reprinted with permission from Feng et al.[14] Copyright 2002, Wiley−VCH Verlag GmbH & Co.KGaA.) (E and F) SEM images of silicon surfaces containing (E) 8 μm × 8 μm four-armed star-shaped posts and (F) 8 μm × 8 μm four-armed square posts. (Reprinted with permission from Oner and McCarthy.[15] Copyright 2000, American Chemical Society.) (G) SEM image of carbon nanotube forests prepared by PECVD with a nanotube diameter of 50 nm and a height of 2 μm (before PTFE coating via HFCVD treatment). (Bar = 1 μm. Reprinted with permission from Lau et al.[28] Copyright 2003, American Chemical Society.) (H) Typical SEM image of a superhydrophobic surface fabricated by packing the flowerlike α-Fe_2O_3 particles. The topography of the surface consists of structures in multiple length scales—the roughness caused by the thin plates, or "petals," on each particle is superimposed onto a larger scale roughness induced by packing the particles. (Bar = 1 μm. Reprinted with permission from Cao et al.[23] Copyright 2007, American Institute of Physics.)

of magnitude of nanometers or micrometers. Furthermore, experimental results are several magnitudes greater than slip length results predicted by simulations (see section III). Simulations enable us to examine the slip length on its microscopic scale, and, most importantly, allow us to compare, on an equal basis, the trends that contact angle and slip length follow. Although current slip length experiments are reviewed herein (see section III.a), emphasis is placed on simulations (see section III.b). Behavior on both smooth (see section IV.a) and patterned surface simulations (see section IV.b) is examined, with respect to contact angle and slip length. The discrepancy between slip length experiments and simulations reported in the literature is also addressed (see section III). An elaborate contact angle−slip length relationship seems to hold, even for simple cases, such as a Lennard-Jones fluid on a graphite surface. Analogous relationships should be explored, to optimize the surface design for more realistic cases, such as patterned surfaces (see section IV.a).

The paper is organized as follows: sections I.a and I.b provide a brief introduction to superhydrophobicity and the characteristics of superhydrophobicity (contact angle and slip length). Section II is focused on the review of simulations for the calculation of contact angles, and section III is focused on calculations of slip length with simulations. Because the slip length is much more difficult to measure than the contact angle, a review of experimental measuring methods is also offered in section III. The connection between slip length and contact angle is explored in section IV, and a predictive method for the slip length and the contact angle is offered in the form of dimensional analysis. The last section (section V) includes the conclusions of the present review.

I.a. Superhydrophobic Surfaces. A superhydrophobic surface is arbitrarily defined as a surface with a contact angle of >150° between the surface and a drop of fluid resting on it[9,10] (although alternative criteria based on contact angle hysteresis, contact line density, and asperity height[11] have been proposed, but not yet widely accepted). Generally, the wettability of a solid surface is a function of its chemical composition and topology. Superhydrophobic surfaces have long been observed in nature, for example, in the self-cleaning mechanism of the sacred lotus leaf (*Nelumbo nucifera*),[12] in the ability of water striders (*Gerris remigis*) to stay on top of a water surface,[13] and in the anisotropic dewetting tendency of a rice leaf.[14]

In the case of the lotus leaf, the complex three-dimensional (3D) microstructure of the leaf, which consists of epidermal cells (papillae) that are covered by hydrophobic epicuticular wax crystals, is responsible for the apparent superhydrophobicity (see Figure 1A). External impurities are picked off of the lotus leaf's surface by a rolling water drop, because drops are not able to adhere to the hydrophobic surface in what is commonly known as the "lotus effect".

A water strider can "glide" on top of water without penetrating its surface due to the extremely hydrophobic nature of its legs. The single leg's amazing hydrophobic properties include the ability to support 15 times the body weight of a water strider (152 dynes), which corresponds to a water displacement of ~300 greater than the leg's volume.[13] Although previously it was believed that this effect is due to surface tension caused by wax secreted on a strider's leg, this phenomenon is not sufficient to account for the leg's superhydrophobicity. Therefore, it is believed that the hierarchical structure (it is composed of numerous needle-shaped microsatae) makes a significant contribution to the hydrophobic behavior of the legs.

The water strider and the lotus leaf are just two examples of many of nature's superhydrophobic surfaces. Another type of superhydrophobic surface found in nature is the patterned surface of a rice leaf (*Oryza sativa).* This type of surface is unique, because a tendency toward anisotropic dewetting has been observed on it.[14] The ordered arrangement of micropapillae is thought to be responsible for this effect. The papillae are arranged parallel to the leaf edge, and randomly in other directions (see Figure 1C).

In an attempt to mimic nature, many artificial superhydrophobic surfaces have been produced (see Figure 1). Such surfaces range from pillar structures and patterned grooves[15] on silicon wafers coated with fluoroalkylsilane (see Figures 1E and 1F), to honeycomb-patterned pin-cushion film made from a fluorinated copolymer,[16] to nonwoven microfabrics,[17] to a copper foil "skin" coated with a solution of fluorosilane in ethanol,[18] to fractal structures made of alkylketene dimers.[19] Amphiphobic surfaces that display both water and oil contact angles of $>160°$ have also been manufactured.[9] A wide variety of other superhydrophobic surfaces has been created artificially, such as artificial lotus leaf surfaces produced by nanocasting (which is based on soft lithography),[20,21] artificial bamboo leaves produced by ultraviolet (UV)-nanoimprint lithography[22] and others. All of these surfaces usually involve some type of chemical surface modification to improve hydrophobicity. Recently, the chemical treatment approach has been criticized for its inability to retain the superhydrophobic properties with time. Non-aging superhydrophobic surfaces have been manufactured without treatments instead (see Figure 1H).[23] Some other examples of superhydrophobic surfaces are those displaying electrowetting,[24] and surfaces whose degree of wettability can be controlled by UV radiation exposure,[25] or by the amount of water in contact with the surface.[26]

The ability to grow carbon nanotubes (CNTs)[27] directly on a substrate using various chemical vapor deposition (CVD) techniques, combined with the ability to functionalize the surface of individual nanotubes, made them attractive material candidates for superhydrophobic surface design (see Figure 1G).[28] Different types of surface patterning are possible, because of the versatility of CNTs (for example, a honeycomb-like aligned CNT film that was grown via the pyrolysis of iron phthalocyanine[29]). Aligned carbon nanotubes (ACNTs) that show superamphiphobic properties have also been prepared by modifying the ACNT film with fluoroalkylsilane.[9]

Three main reasons are believed to be responsible for the repulsion of a fluid by a solid: (a) chemical treatment of the solid surface, (b) surface roughness, and (c) presence of nanobubbles between the solid and the liquid. (Other factors that affect hydrophobicity under special circumstances include electrowetting,[24] and solid and liquid impurities[30,31]). Characterization and influences of wettability, new development methods for superhydrophobic surfaces from both experimental and theoretical aspects, and the prospects of new applications of superhydrophobic surfaces have been recently reviewed.[32] Similarly, preparation approaches, including advantages and limitations of different strategies, and problems/obstacles related to the utilization of superhydrophobic surfaces in real life have also been reviewed.[33]

Figure 1 is a collage of various natural and artificial superhydrophobic surfaces.

Chemical Modification of the Surface. Most commonly, the chemical modification is fluorination.[19,24] A classic example is one of a vertically aligned CNT forest, deposited with a plasma-enhanced chemical vapor deposition (PECVD) technique.[28] The effects of chemical modifications on fluid flow over the treated surface have been studied experimentally by several researchers, such as Baudry et al.,[34] Tretheway and Meinhart,[35] and Choi et al.[36]

Surface Roughness. Two mechanisms are thought to be responsible for roughness-induced hydrophobicity. The first mechanism is associated with the fluid−solid configuration known as the Cassie state.[37] In this state, air is trapped in the surface roughness between the liquid and the solid, such that the liquid is partially floating on air. The second mechanism is associated with the Wenzel state.[38] In this model, hydrophobicity is increased because the surface area of the rough solid is much greater than that of a flat surface, so the interfacial energy is increased. The Cassie state is generally preferred over the Wenzel state in superhydrophobic surface design, because of the former's smaller solid−liquid contact area. Some Wenzel−Cassie intermediate regimes have been observed via simulation, signifying that these two states correspond to limiting configurations.[39] Control of the transition from the Cassie state to the Wenzel state has been achieved by varying the topology parameters of the surface, such as height and spacing of the roughness.[12,40] It has been determined that the stability of the Cassie state is lost above an interfacial pressure on the order of $\Delta P_{int} \approx 2\gamma_{LV}/R$ (where R is the characteristic roughness scale).[41] Recently, it has been suggested that, for a Cassie state, the curvature of the liquid surface into the roughness gaps is the cause of two counteracting effects on the effective slip length. One is due to the change in the cross-sectional area of the flow passage (and, therefore, an increase or decrease in flow rate), and the other is due to the change of the fluid velocity field (residual nonzero shear stress is introduced by the curvature).[42] In principle, control of the curvature would permit some control of the slip length. Finally, a strategy has been proposed to optimize roughness for superhydrophobicity by maximizing suspension pressure and minimizing drop retention.[10]

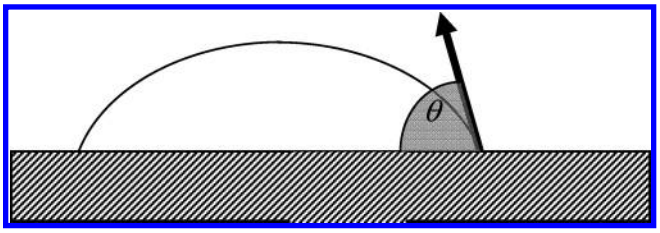

Figure 2. Schematic of a drop of liquid in equilibrium with a solid surface, surrounded by vapor. The contact angle is shown as θ. (Reprinted with permission from Voronov.[48] Copyright, University of Oklahoma, 2006.)

Nanobubbles. Approximately in the mid-1990s, experimental evidence of the existence of small amounts of gas trapped on rough and/or hydrophobic surfaces began to grow; this growth was due to the availability of high-precision experimental techniques.[30] A conceptual picture of nanobubbles covering a solid surface is that of a heterogeneous surface with regions of liquid flowing over gas, and of liquid flowing over solid. Some of the recent examples of experimental observations of nanobubbles in water on hydrophobic surfaces, via tapping-mode atomic force microscopy (AFM), include works by Ishida et al.,[43] Tyrell and Attard,[44] and Steitz et al.[45]

I.b. Characteristics of Hydrophobicity. Contact Angle. Experimental measurement of the contact angle can be essential for several industries: printing, semiconductors, cosmetics, biology, lacquers and paints, preservation of buildings, environment, medical field, optics, dental materials, paper industry, polymers, synthetic foils, textiles, adhesives, etc. The contact angle is a macroscopic quantity that is easily measured in the laboratory and is an indicator of wetting. The contact angle and related wetting issues have been thoroughly reviewed by other researchers.[46,47]

The contact angle (depicted in Figure 2) is geometrically defined as the angle on the droplet side of the line tangent to the liquid−vapor interface, drawn through the three-phase boundary. For a three-phase system, where two of the phases are fluidlike (most commonly, a liquid and a vapor) and the third phase is a solid, Young's law[49] describes the relationship between the contact angle and the solid−vapor, solid−liquid,

and liquid−vapor interfacial tensions. A fluid displaying wetting behavior has a contact angle of $0° \leq \theta \leq 90°$, whereas a fluid that displays nonwetting behavior has a contact angle of $90° \leq \theta \leq 180°$. In the case of microscopic droplets, an additional free energy per unit length or line tension (τ) contributes to the excess free energy of the droplet. Because of the solid−liquid−vapor contact line length, an additional term appears, which leads to the modified Young's equation:[50]

$$\gamma_{SV} = \gamma_{SL} + \gamma_{LV}\cos\theta_{\infty} = \gamma_{SL} + \gamma_{LV}\left(\cos\theta + \frac{\tau}{R\gamma_{LV}}\right) = \gamma_{SL} + \gamma_{LV}\cos\theta + \frac{\tau}{R} \quad (1)$$

Curiously, however, Young's Law has never been verified experimentally (because measurement of the surface tension of solids is difficult), despite its wide acceptance.[47] Modifications of Young's Law have been developed in cases of nonuniform surfaces (such as that in the Wenzel and Cassie states), fractal-type microroughness coverage of rough surfaces (similar to a Koch curve),[14] composite surfaces consisting of different small patches, and meshlike surfaces.[47] Other contact angle models include the Girifalco−Good−Fowkes−Young (GGFY) equation,[47] which is based on a semiempirical determination of the contact angle of two mutually immiscible van der Waals phases, and the Potential Distortion Model, which is based on isotherms.[47,51] For the case of very "soft" solids, elastic deformation can make a substantial contribution to the wetting behavior of the solid surface.[52,53] Accounting for the softness requires compensating for the normal component in the force balance, which yields the augmented Young−Laplace equation for the contact angle.[54]

Experimental techniques for measuring the contact angle can be divided into two main categories: those based on goniometry and those based on tensiometry. Some examples of these techniques are tilting plate, sessile bubble and drop, captive bubble, dynamic and single fiber wilhelmy, and powder contact angle methods.[47] Experimentally, the value of the static contact angle is determined to be dependent on the recent history of the interaction. If the drop has recently expanded, the angle is said to be "advanced" and, if it contracted, the angle is said to be "receded". The angles correspond to the maximum and minimum limits, respectively. If the droplet is in motion, the dynamic contact angles are referred to as "advancing" and "receding", and are dependent on the relative speed between the substrate and the contact line.[55] The difference between the maximum and the minimum contact angle values is called hysteresis (other types of hysteresis also exist[56,57]). Contact angle hysteresis can occur due to two major reasons: (i) surface roughness or (ii) surface and liquid contaminants/inhomogeneities, which can create barriers to motion of the contact line. Hysteresis has been used to characterize surface heterogeneity and the ability of a drop to move on such a surface. A smaller contact angle hysteresis is considered to be one of the defining characteristics of a superhydrophobic surface. However, in simulations, where gravitational and impurity effects are neglected, the droplet can be assumed to be a perfect sphere (free of hysteresis) and the microscopic contact angle can be measured directly from equations that have been developed based on geometric principles.[48] Although we focus on the static contact angle herein, research is ongoing to understand phenomena that involve dynamic contact angles. Important issues include the connection between static and dynamic wetting properties;[58−60] viscosity effects,[61] surface contamination effects,[60] flow field, and geometry;[62] the relationship between roughness effects and dynamic wetting;[63] and the process of dewetting.[64−66]

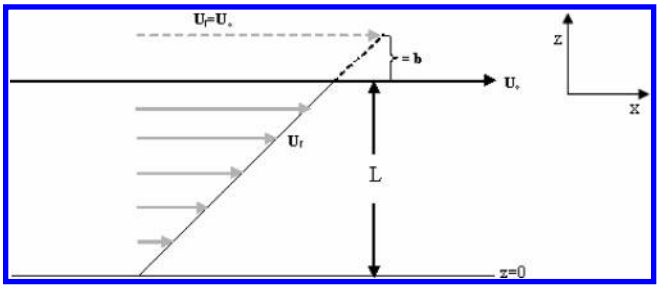

Figure 3. Definition of the slip length b in a planar Couette flow. Upper wall moves at U_o, while the lower wall is fixed. (Reprinted with permission from Voronov et al.[74] Copyright 2006, American Institute of Physics.)

Slip Length. A direct effect of hydrophobicity in fluid dynamics is that fluid can slip past a solid hydrophobic surface (similar to flow past another fluid[67]). The slip length is a microscopic quantity that can be used to quantify hydrophobicity. It is also an indicator of drag reduction. However, to this day, it is very difficult to measure slip length experimentally, and analytical predictions have been just as elusive. To address this bottleneck in science, a textbook simplification called the "no-slip" boundary condition was proposed and soon thereafter widely accepted during the early stages of continuum fluid dynamics. This condition means that fluid molecules at the immediate surface of a solid move with exactly the same velocity as that of the surface. Fluid mechanics has long relied on this assumption to successfully model many macroscopic experiments where slippage effects can be deemed negligible.[68] While the no-slip boundary condition has been proven experimentally to be accurate for several macroscopic flows, it remains an assumption that is not based on physical principles and leads to singular or unrealistic behavior in cases of liquid spreading on a solid substrate, corner flow, and extrusion of polymer melts from a capillary tube.[69] Reported evidence of slip includes the flow of water past hydrophobic surfaces and the "weak link" argument (stating that either slip or breakdown of the fluid must occur as the shear rate approaches infinity): both make a valid case against the no-slip boundary condition.[70] In addition, the no-slip boundary condition implies a divergent energy dissipation rate in the case of a contact line that separates two immiscible fluids moving along a solid surface.[71] Growing evidence[72] that fluids flowing past hydrophobic surfaces experience slip at the boundary, manifested especially at the microscopic scale, has been accumulating. In fact, ~200 years ago, Navier proposed a general boundary condition that incorporated the possibility of fluid slip at a solid boundary. Navier's proposed boundary condition assumed that the velocity U_x at a solid surface is "proportional to the shear stress at the surface".[35]

For planar Couette flow, the slip length (b) is defined as the distance inside the wall at which the extrapolated fluid velocity would equal the velocity of the wall (the inverse of parameter ϵ in Navier's work[73]). The situation is depicted in Figure 3, for the case where one wall moves at a uniform speed U_o and the bottom wall is stationary. The actual fluid velocity at the wall (U_f) lagging behind U_o during slip is extrapolated outward into the walls using a constant wall shear $dU/dz|_0$ over a distance b, where it catches up with U_o. This distance is called the slip length. It would be equal to zero if the fluid did not slip (i.e., if the fluid stuck to the wall and its velocity U_f were equal to U_o at $z = L$).

The slip length is mathematically defined as

$$b = \frac{U_o - U_f|_{z=L}}{(\partial U_f/\partial z)|_{z=L}} \quad (2)$$

For forced-flow types, such as the Poiseuille flow, the slip length can be related to an external force driving the flow. An alternative definition of slip length that relates it to the hydrodynamic force has also been introduced, but it is not used in this study.[75,76]

With regard to slip, one must distinguish between true slip and apparent slip.[70] In both cases, the bulk fluid velocity effectively "slips" at the wall. For *true slip*, the fluid close to the wall actually moves with a different velocity from the wall. In the case of *apparent slip*, a low-viscosity component in the fluid creates a larger velocity gradient near the surface. The velocity gradient in this layer is so high that the fluid on top of the zone seems to slip by the wall, although the actual slip occurs at the fluid/fluid interface, not at the solid/fluid interface. No experiment exists at this time that would be able to distinguish between the two types of slip. In the case of non-Newtonian fluids (polymer melts and concentrated solutions), there are three mechanisms for wall slip: (a) slip is the result of an adhesive failure of the polymer chains at the solid surface; (b) slip is a cohesive failure resulting from disentanglement of chains in the bulk from chains adsorbed at the wall, so that polymer is slipping over an adsorbed "brush"; and (c) there is a lubricated layer at the wall (perhaps the result of a stress-induced transition to a low-viscosity mesophase).[77]

The magnitude of slip at a fluid/solid boundary is of interest to many fields of research, including microfluidics devices, fluid flow through porous media and in biological systems, drainage flow between particles in mutual motion, contact line motion of fluid interfaces, and, generally, friction and wear. If the large slip lengths (on the order of micrometers) that have been reported for some experimental systems are correct, then modifications to the classical hydrodynamic theory may be required.[78] Furthermore, significant drag reduction savings have been predicted for large slip lengths in turbulent flows numerically[3] and theoretically.[6] It is noteworthy to mention that the effects of slip in turbulence are dependent on the direction of the slip.[3,6] Stream-wise slip increases drag reduction, and span-wise slip decreases it. In other words, not all slip is beneficial for drag reduction applications!

Typically, solids are artificially modified to create superhydrophobic surfaces, such as those discussed in section I.a, to achieve a large slip length. Alternatively, the fluid itself can be doped with a friction reducer, such as a surfactant, to achieve slip.[79] In both cases, however, the fluid−solid interphase is modified, because slip is an interphase phenomenon. For a further review of the experimental techniques for measuring slip length, see Neto et al.;[30] for an overview of analytical studies and simulations of the slip length, see Priezjev and Troian.[80] Furthermore, a wide range of no-slip boundary condition issues has been recently reviewed by Lauga et al.[81]

I.c. Oversimplification by Conventional Wisdom. Conventional wisdom presumes that a higher contact angle leads to a greater slip length.[4,82,83] In fact, when materials scientists search for surfaces with friction−drag reduction potential, a high contact angle is the main criterion for success.[16,20,82] However, the use of the contact angle to judge hydrophobicity has been criticized, because it does not account for dynamic effects, such as how much force is required to move a droplet on a surface.[15] In fact, evidence exists that it is possible for slip length to decrease with higher or constant contact angle.[74,84] Furthermore, geometrical roughness aspects (such as anisotropic patterns, roughness height, and pattern wavelength) can also have different effects on the contact angle and the slip length.[48]

II. Calculating the Contact Angle with Simulations

Although not experimentally verified, Young's law is used as the formal definition for contact angle by a prevailing number of researchers. Its modifications exist for heterogeneous surfaces; however, they correspond to limiting cases and do not account for relative droplet size, surface geometry, or effects of sharp corners on the contact line. Experimental measurements of the contact angle for different systems are abundant, but they can be tainted by the reduction of surface tension by gas contaminants, solid surface impurities and defects, and large contact angle hysteresis.[85] In light of these drawbacks, simulations present a valuable tool to explore contact angle behavior. However, computing power today allows for the modeling of droplets on the order of nanometers in size. Equilibrium molecular dynamics (EMD) has been used to study the contact angles. (Extensive work on simulating contact angles using EMD has been presented in a dissertation by Sinha,[86] as well as by others.[87−94]) Solid walls on which the droplet is situated were historically modeled as a face-centered cubic (FCC) lattice, and, for convenience, the fluid itself was typically modeled as a simple Lennard-Jones fluid. Currently, the modeling of other practical solids and liquids (water on graphite, for example) is becoming more popular. Modeling complex liquids, such as water, however, presents somewhat of a difficulty, because of the elusive nature of the energy potential functions and complex 3D structures that the molecules form.

As stated previously, for simplicity and realism, the early contact angle simulations were performed with a monatomic fluid wetting an FCC-type substrate, using a Lennard-Jones (LJ) potential to model the interparticle interactions as follows:

$$\Phi_{ij}(r) = 4\epsilon_{ij}\left[\left(\frac{\sigma_{ij}}{r}\right)^{12} - \delta\left(\frac{\sigma_{ij}}{r}\right)^{6}\right] \quad (3)$$

where r is the distance between the particles, ϵ_{ij} and σ_{ij} are the potential well depth and the atom size parameter. The Lennard-Jones equation consists of a repulsive 12th-power term and an attractive 6th-power term. The repulsion term that describes electron repulsions has no theoretical justification, whereas the attractive term is derived from dispersion interactions. The equation is a particularly good approximation for noble gases, such as argon, as well as for neutral atoms and molecules. The terms ∂ and δ are artificially introduced into the LJ equation by some authors, to vary the attractive/repulsive properties of the solid substrate.

Saville[87] is one of the pioneers of contact angle simulations. He simulated fluid molecules interacting among themselves with a 6−12 Lennard-Jones potential and with an external solid 3−9 Lennard-Jones potential. Saville attempted to measure the contact angle directly and by computing it from surface tension values according to Young's Law; however, no satisfactory agreement was achieved between the two types of measurements. He observed that the contact angle decreased as the wall density increased, which is equivalent to increasing the relative strength of the solid−fluid interactions (ϵ_{sf}), according to his derivations. No wetting or drying transitions were observed in that study, although the possibility for them to occur was left open at extreme fluid−solid interaction values. Later, Sikken et al.[95] simulated both wetting and drying transitions for a similar

system. Nijmeijer et al.[89] developed a formula, based on minimization of free energy, that allowed the authors to measure the contact angle directly by fitting the shapes of the equidensity lines to a circle. Both Sikken et al.[95] and Nijmeijer et al.[89] verified that the contact angle increases as ϵ_{sf} decreases. In a dissertation by Sinha,[86] it was observed that the contact angle increases with lower ϵ_{sf}, σ_{sf}, or T. Thus, contact angle behavior as a function of each one of the LJ parameters appearing in eq 3 was established, completing the picture for these simple systems.

The next challenge, and milestone, in contact angle simulations, was to implement complex fluid systems. Thompson and Robbins[96] attempted to model two immiscible monatomic Lennard-Jones fluids that were confined between solid walls and sheared by them. The dynamic contact angle was measured, and it was determined that it is consistent with macroscopic theories. Obtained flow fields were consistent with solutions of the Navier−Stokes equation with an exponentially decaying slip boundary condition, which occurs within two fluid diameters of the contact line. Bertrand et al.[64] investigated dynamics of spontaneous wetting by modeling eight-atom LJ chains on a planar square lattice. Their results implied not only that the mobility of the liquid molecules adjacent to the solid increases with decreasing solid−liquid interactions, but also that the mobility adjacent to the free surface of the fluid is higher than in the bulk.

Water is generally the fluid of interest in practical applications, and, ironically, it is one of the most challenging fluids to model. Over 46 water potential models exist today, but none of them completely accounts for all physical properties of water.[97] Among the simplest models that reproduce most of the water properties accurately (although they do not require extensive computer resources) are the Simple Point Charge-Extended (SPC/E)[98] and the Transferable Intermolecular Potential−3-Point (TIP-3P)[99−101] models. Hautman and Klein[102] simulated water molecules on a surface consisting of long-chain alkylthiol molecules on a gold substrate. Tail groups on the self-adsorbed monolayer formed on the gold surface were changed from CH_3 (represented by a spherical pseudo-atom) to OH, to simulate a hydrophobic and hydrophilic surface, respectively. Contact angle measured on a hydrophobic surface was determined to be 135° at 300 K and decreased to 120° at 200 K. For a hydrophilic surface, the contact angle was in the range of 5°−17°. A similar study by Mar and Klein[103] measured the contact angle of 80 *n*-hexane molecules on the same type of hydrophobic surface to be 60° at 300 K.

Recently, the carbon−water and the water−CNT interactions have received much attention, because of the hydrophobic properties of graphite and a growing interest in CNTs. The simplest approach to modeling carbon−water interactions is to use mixing rules,[104−110] in conjunction with the aforementioned simple water models. Custom[111] and tuned[112,113] water-graphite potentials that reproduce experimentally observed contact angles also exist. In the first of a series of three papers by Koumoutsakos et al. that was dedicated to this subject, the C−O Lennard-Jones well depth (ϵ_{CO}) was tuned in order to recover the macroscopic contact angle for a graphite-water system.[112] The authors considered a multitude of previously used potentials and ended up tuning the SPC/E model, without considering C−H interactions. In the second paper of the series, the C−O Lennard-Jones well depth (ϵ_{CO}) was tuned to recover the macroscopic contact angle while compensating for line tension effects. Also, a continuum model for graphite was proposed, and effects of adding C−H Lennard-Jones interactions and those of changing the long-range Coulomb cutoff were explored for both discrete and continuum graphite models.[113] It was found that the effect of long-range cutoff of the LJ potential is negligible for the continuum model, but is significant for the discrete one. The effect of adding LJ interactions between graphite and hydrogen atoms was also determined to be significant. Finally, the third paper of the series considered effects of fluid and surface impurities on water−carbon interactions.[31] It was determined that the contact angle decreases weakly with increasing ionic concentration in the water, but the influence of solid impurities is more significant: the contact angle decreases with increasing coverage of chemisorbed hydrogen.

Lundgren et al.[108] used a TIP-3P model to model a water droplet on a single sheet of atomistic graphite. By changing the surface characteristics from hydrophobic to hydrophilic, a range of contact angles with higher contact angles corresponding to a lower ϵ_{CO} were observed. In addition, impurity effects were explored by adding ethanol to the water, as a result of which the contact angle decreased. Peculiarly, the ethanol molecules were concentrated close to the solid surface and at the water/vapor interface, with the polar heads pointing toward the center of the droplet. Janecek and Netz[114] measured interfacial tension (and thus the contact angle), as well as structural properties of water on a rigid substrate (such as the depletion layer thickness and preferred water orientation), while changing the arrangement of interaction sites in the lattice (hexagonal versus square), the dispersive interaction strength, and the density of polar groups in the surface layer of the solid phase and their orientation and spatial distributions. The main conclusion obtained from their Monte Carlo simulations was that, for a given temperature, a universal relationship between the depletion thickness and the contact angle seems to exist.

Modeling the Cassie and Wensel states on rough surfaces is a current topic of interest for many simulationists. Cao et al.[115] modeled the contact angles on surfaces with an array of nanoscale triangular roughness of variable affinity for the fluid. Table 1 is a summary of the simulations previously discussed. Note that simulations on complex surfaces are further discussed in section IV.b.

III. Measuring Slip Length Experimentally and with Simulations

The existence of slip length was postulated over a century ago; however, because of technological constraints, it could be neither verified nor disputed unequivocally. A wide spectrum of boundary conditions, including slip, was simulated using molecular dynamics techniques in the early 1990s. As high-resolution imaging techniques and other innovative experimental methods became available, several attempts were made to measure the slip length. It is now generally accepted (although some controversy persists[117]) that the slip is a real physical phenomenon; experimental observations of this phenomenon date back as far as the 1960s via experiments on polymer melts.[77,118] However, the experimental measurements still suffer from poor resolution and contamination. Simulations can offer instrumental support in the interpretation of the detailed mechanisms of interfacial slip. However, a persistent discrepancy exists between experiments and simulations, in regard to the order of magnitude of slip: simulation results suggest it to be on the order of magnitude of several angstroms to nanometers, whereas experiments and theory[119] estimate it to be on the order of micrometers. According to computational fluid dynamics (CFD) experiments, the latter would be significant for drag reduction, whereas the former would not.[3]

Table 1. Summary of Simulation Findings about the Calculation of the Contact Angle

	Fluid		Solid			
author	fluid type	number of atoms	solid type	number of atoms	parameter varied	contact angle (°)
Saville[87] (1977)	monatomic LJ	255−1205	semi-inf. FCC 3−9 LJ		ρ_s	45−140
Sikken et al.[95] (1987)	monatomic LJ	8500	rigid FCC	2904	ϵ_{sf}	0−180
Nijmeijer et al.[89] (1989)	monatomic LJ	8064	rigid FCC	2904	ϵ_{sf}	0−180
Thompson et al.[96] (1989)	monatomic LJ	1344	vibrating FCC	672	shear rate, number of fluid particles	105−165[a]
Sinha[86] (2004)	monatomic LJ	1000	semi-inf. FCC 3−9 LJ		ϵ_{sf}, σ_{sf}, T	0−115
Cao et al.[115] (2006)	monatomic LJ	8900	vibrating FCC smooth or with isosceles triangular grooves	6000	isosceles side length, ϵ_{sf}	36−165
Bertrand et al.[64] (2007)	8-atom LJ chains		vibrating square planar lattice		∂ and δ	101.6−143.8
Cieplak et al.[116] (2006)	LJ chains/FENE	1800	vibrating FCC, energetic patches		δ	130
Hautman and Klein[102] (1991)	water	90	$SH(CH_2)_{11}X$ on gold, where $X = CH_3$ or OH	90	head group X, T	5−135
Lundgren et al.[108] (2002)	TIP-3P water	1000	one layer graphite		ϵ_{CO}, liquid impurity	30−150
Part I: Koumoutsakos et al.[112] (2003)	SPC/E, TIP-3P water	2000−17576	two layers of fixed or vibrating graphite		water models, drop size, ϵ_{CO}	42 and 86
Part II: Jaffe et al.[113] (2004)	SPC/E water	2000	fixed graphite and semi-inf graphite	10752 (fixed graphite)	long-range LJ cutoff, C−H LJ interactions, ϵ_{CO}	27.6−180
Part III: Walther et al.[31] (2004)	SPC/E water	2000	fixed graphite	10752	solid and liquid impurities	60−90
Janecek and Netz[114] (2007)	SPC/E water	1420	fixed hexagonal/tetragonal with hydroxyl groups		lattice, interaction strength, hydroxyl density/orientation	130

[a] Dynamic contact angle values.

III.a. Experimental Slip Length Measurements. Slip is a phenomenon that occurs on a scale of a few nanometers to a few micrometers. Therefore, extremely accurate techniques that are capable of measuring interfacial flow at such scales are required to detect slip. The most important techniques can be broken down into four main categories: (a) techniques tracing the fluid flow near a boundary (fluorescent recovery after photobleaching, particle image velocimetry); (b) techniques based on force or displacement measurement (surface forces apparatus,[120,121] atomic force microscopy (AFM)[122,123]); (c) capillary techniques; and (d) quartz crystal resonators (quartz crystal microbalance).[30,124] Other methods that have been used to measure slip include studying flow of thin films on spinning disks and on rotating cylinders, droplets moving down an inclined plane surface, particle sedimentation rates, and excitation of surface waves.[30] Many different experimental techniques were developed to measure the slip length, but few of them can measure it directly, without making any assumptions.

Techniques tracing the fluid flow near a boundary are among the few examples that measure the slip length directly. Although, recently, questions have been raised about the validity of the slip observed with total internal reflection velocimetry (TIRV), due to electrokinetic effects[125] and electrostatic repulsion effects[81] between tracer particles and the solid surface, the results of the TIRV techniques are still worth discussing. For example, TIRV was combined by Jin et al.[126] with evanescent wave illumination of sub-micrometer particles to measure the slip velocity of water flowing past glass coated with an octadecyltrichlorosilane (OTS) monolayer. Pit et al.[127] also used a tracing technique in a novel experiment using total internal reflection−fluorescence recovery after photobleaching (TIR-FRAP) to probe the velocity of a liquid near a wall for a hexane stearic acid mixture. It was found that chemical modification of a sapphire surface via the adsorption of stearic acid modifies the boundary condition of shear flow of hexadecane from no-slip to slip. Schmatko et al.[128] used near-field laser velocimetry (NFLV), which also is based on TIRV after photobleaching, to demonstrate that small changes in the shape of the molecules of the fluid can facilitate wall slip in the case of linear elongated cigar-shaped molecules or, in contrast, decrease the aptitude to slip in the case of branched molecules by as much as a factor of 3, when compared to linear molecules. Moreover, they confirmed that a totally wetting surface can lead to noticeable slip at the wall. Huang et al.[129,130] used TIRV to show that variations in the aqueous ionic concentration do not change measured slip lengths significantly, which consequently suggests that true boundary slip is, in fact, what is being measured.

Other researchers also observed the effects of surface hydrophobicity on the slip length. Choi et al.[36] indirectly measured the slip length in a channel with hydrophobic and hydrophilic coatings. Although some experimental error was present, it could be concluded that (a) significantly more slip occurred in the channel with a hydrophobic coating, and (b) the slip length varied linearly with shear rate in both channel types. Zhu and Granick[131] showed that slip length is higher for fluid−solid pairs with higher contact angles. A surface force apparatus (SFA) with three fluid−solid layers was used to show this trend.

In an alternative experimental setup, the fluid was varied instead of the solid surface, to observe hydrophobicity effects on the slip length. Majumder et al.[132] measured the velocity of several different pressure-driven fluids flowing through a multiwalled CNT membrane 7 nm in diameter. An ordered hydrogen-bonded network and a weak attraction between water and the smooth CNT graphite surface were credited for slip lengths higher than those predicted by conventional fluid flow theory. The flow velocity was determined to increase for more-hydrophilic fluids (lower slip length for hydrophobic solvents), but did not increase with higher fluid viscosity. Materials supplementary to their paper contain data for 0.017 M KCl with a corresponding slip length of 108 μm.

Recently, Honig and Ducker[117] found that a smooth solid/liquid interface for a liquid that has strong interactions with the solid results in the no-slip boundary condition casting doubt on previous measurements of slip length. However, even they

Table 2. Summary of Experimental Measurements of the Slip Length

author	fluid type	solid substrate	method/variable	slip
Pit et al.[127] (1999)	hexane + stearic acid (1%)	Al_2O_3	TIR-FRAP	0−275 nm
Craig et al. [124] (2001)	aqueous solution of sucrose (BDH, AR)	gold coated mica w/ self-assembled monolayer from a 10 mM 11-mercapto-1-undecanol and 10 mM 1-dodecanethiol (20% dodecanethiol) in ethanol	AFM/shear rate, viscosity	0−20 nm[a]
Zhu et al.[131] (2001)	deionized water, tetradecane	octadecyltriethoxysiloxane (OTE), mica	SFA/fluid-solid, shear rate	0−2.5 μm[a]
Choi et al. [36] (2003)	pure water	polished Pyrex wafer, self-assembled layer of octadecyltrichlorosilane on silicone	capillary/wall hydrophobicity or hydrophilicity	−3−35 nm
Neto et al.[135] (2003)	aqueous solution of sucrose (BDH, AR), linear-chain polydimethylsiloxane (PDMS)	gold-coated w/ self-assembled monolayer from 11-mercapto-1-undecanol and 1-dodecanethiol, silica/silicone oxide	AFM/fluid type and viscosity, solid type, shear rate	0−190 nm
Jin et al.[126] (2004)	water	glass coated with octadecyltrichlorosilane (OTS) monolayer	TIRV−TIRFM−PTV/shear rate	<10 nm
Majumder et al.[132] (2005)	water, ethanol, *i*-propanol, hexane, decane	MWCNT membrane	capillary/fluid type	3.4−68 μm
Schmatko et al.[128] (2005)	squalane and hexadecane	AlO_3, SiH, OTS	NFLV/fluid and solid types	50−350 nm
Cottin-Bizonne et al.[133] (2005)	water, dodecane	plain Pyrex and Pyrex/OTS	dSFA/fluid and solid types	0−20 nm
Choi et al.[7,134] (2006)	water, 30 wt % glycerin	conical posts, grooves on silicon wafer	cone-and-plate rheometer/shear rate, fluid and coating types	0−50 μm
Joseph et al.[41] (2006)	DI water with markers	CNT forest on SiO_2-silicone	μ-PIV/roughness scale	0−1.5 μm
Huang et al.[129] (2006); Huang et al.[130] (2007)	DI water with markers, aqueous NaCl solutions	polydimethylsiloxane (PDMS) on glass wafers, oxygen plasma treated or coated with octadecyltrichlorosilane (OTS)	3D−TIRV/NaCl concentration, coating types, shear rate	25−100 nm
Truesdell et al.[136] (2006)	not specified (Newtonian)	polydimethylsiloxane (PDMS)	PIV/patterning, coating, layer thickness	up to ~250 μm
Cross et al.[137] (2006)	water	dipalmitoyl phosphatidylcholine (DPPC) phospholipids	dSFA/immersion time	0−10 nm
Honig and Ducker[117] (2007)	aqueous sucrose solution	glass	AFM/solution viscosity, drive rate	−5−1.5 nm

[a] Slip length definition is according to Vinogradova.[75,76]

postulated that slip might be expected to occur when the interaction between the solvent and solid are weaker. Cottin-Bizonne et al.[133] attempted to measure intrinsic slip length, i.e., one that is free of artifacts such as gas trapped at the liquid/solid interface or surface contamination. They observed no slip on perfect and partial wetting configurations, whereas significant slip was observed in the nonwetting situation with water flowing on a smooth hydrophobic surface.

Other experiments suggest that the slip length might be a function of parameters other than just solid−fluid interactions. Craig et al.[124] used AFM to directly measure the hydrodynamic drainage forces of an aqueous Newtonian fluid bounded by a relatively hydrophilic solid surface. It was determined that slip length is a function of both surface approach velocity and fluid viscosity. A higher viscosity and higher driving rate resulted in a greater slip length. Choi and co-workers[7,134] experimentally verified that the slip length is proportional to the fluid viscosity. Also, directional control of the slip was demonstrated by comparing the flow of water parallel and transverse to grooves on a silicone wafer, with the parallel configuration consistently having a significantly larger slip length. Neto et al.[135] studied the flow of Newtonian and polymeric liquids by AFM. Their force measurements revealed clear evidence of boundary slip and showed that the degree of boundary slip is a function of the liquid viscosity and the shear rate.

Choi and co-workers[7,134] also showed that surface roughness is another important parameter that influences the amount of slip and that it could be optimized on a micrometer scale to obtain slip lengths at least 2 orders of magnitude greater than that of nonoptimized surfaces. On a surface made of conical posts on a silicone wafer, slip lengths as large as 20 and 50 μm were obtained for a laminar flow of water and for a laminar flow of 30 wt % glycerin, respectively. For Couette flow between two parallel plates with a 10-μm separation, these were translated as 66% and 83% drag reduction. Joseph et al.[41] used micro-PIV to verify that the slip length is proportional to the characteristic lateral roughness scale, as was previously suggested by theory, by experimental investigation of liquid flow slippage over superhydrophobic surfaces made of carbon nanotube forests. Truesdell et al.[136] used PIV to show that, for low-Reynolds number shear flow between two surfaces, one of which has a regular grooved texture augmented with a superhydrophobic coating, the slip length is a factor of ~10 greater than the groove size (25 μm), leading to drag reduction on the order of 20%.

Cross et al.[137] showed that slippage past a solid surface could have an important role in biological applications by studying flow past phospholipid films (model structures for studying properties of native biological cell membranes and to investigate biological processes). They investigated monolayers and bilayers of DPPC (dipalmitol-phosphatidyl-choline) deposited on clean hydrophilic float Pyrex surfaces by dynamic surface force apparatus (dSFA).[120] A significant slip of 10 nm was found on fresh monolayers (which are strongly hydrophobic), though it disappeared after 1 day of exposure to water, because of the increased hydrophilicity and roughness of hydrated monolayers, as was hypothesized by the authors.

In summary, recent experiments have shown that the amount of slip is controlled (a) by the relative affinity of the solid of the fluid flowing past it, (b) by the fluid viscosity (or by a thin stratum of liquid of lower viscosity formed next to the wall) and the surface approach velocity, and (c) by the trapping of gas by surface roughness and through the directional orientation of the roughness. Although numerous experimental slip length studies have been performed, there is still a debate in the literature as to whether slip exists on wetting surfaces. Table 2 summarizes the experiments previously discussed.

Other factors that have been experimentally observed to affect the slip length are the shear rate, curvature of the solid boundary, and polarity of the liquids. For an in-depth review of experi-

mental slip length measuring techniques and their findings, see Neto et al.[30] and Lauga and Stone.[81]

III.b. Calculating Slip Length with Simulations. It is rather routine practice to calculate the slip lengths directly using molecular simulations, but the obtained results are several orders of magnitude lower than those measured by experiments. Nonequilibrium molecular dynamics (NEMD) has been used for both Couette flow and Poiseuille flow to study slip,[138,139] as well as the lattice Boltzmann method.[140−142] The definition of slip length[73] used to compute it in simulations is the one depicted in Figure 3. Most of the studies use a Lennard-Jones[143] type interaction (eq 3), because of its simplicity, where one or more of the LJ parameters are varied to explore the effects on slip. The term δ in eq 3 is artificially introduced into the LJ equation by some authors in hydrophobicity studies, to vary the affinity of a solid substrate to a fluid.

The pioneering work of Koplik and Banavar[144] showed that molecular dynamics simulations can successfully reproduce the continuum properties of low-*Re* flow near realistic solid boundaries, such as velocity and stress fields consistent with the solutions of the Stokes equations. The molecular dynamics simulations were used as a tool to examine the validity of the continuum level no-slip boundary condition at the microscopic level. In a dense fluid, the no-slip boundary condition emerged without any explicit assumptions, whereas at lower fluid densities, such as those in the case of rarefied gases, slip was observed. Moreover, it was shown that the no-slip condition failed at a moving contact line between two immiscible fluids, thereby reconciling the divergent energy dissipation rate issue that was previously mentioned in section I.b.

Thompson and Robbins[145] found a broad spectrum of boundary conditions, including slip, stick, and locking using molecular dynamics. Locking is the opposite of slip. It is supposed to occur when the fluid velocity equals that of the several wall layers inside the fluid. In other words, the fluid layers become interlocked to the layer closest to the wall and all of the locked fluid layers move with the speed of the wall, producing a negative slip, as opposed to the no-slip condition when only the closest layer to the wall moves with the wall velocity. At large ϵ_{wf}, epitaxial ordering was induced in the first two layers of fluid normal to the wall. The no-slip condition occurred for systems with equal wall and fluid densities. Positive slip was only achieved at very weak ϵ_{wf}. Thomson and Troian's[69] data also suggest that lower ϵ_{wf} and commensurate fluid−wall densities produce higher slip.

Nondimensional versions of the LJ parameters, dubbed as the relative energy parameter (ϵ_r), and the relative atom size (σ_r) are defined as follows:

$$\epsilon_r = \frac{\epsilon_{sf}}{\epsilon_{ff}} = \sqrt{\frac{\epsilon_{ss}}{\epsilon_{ff}}} \tag{4a}$$

$$\sigma_r = \frac{\sigma_{sf}}{\sigma_{ff}} = \sqrt{\frac{\sigma_{ss}}{\sigma_{ff}}} \tag{4b}$$

where the subscripts s and f are used to denote the solid and the fluid, respectively. Few MD studies have explored how slip length varies with σ_r, whereas many have addressed the effects of ϵ_r and δ. Recently, Galea and Attard[78] performed a calculation to investigate the effects of atomic-scale roughness on the slip behavior for LJ fluids. The effects of the wall/fluid and fluid/fluid interactions on the slip length, from the size ratios (σ_r = 0.8−1.2), were investigated. This ratio measures the surface roughness that is due to atomic size differences. It was reported that the slip length can display a minimum for commensurate fluid−solid sizes. The authors concluded that epitaxial layering has no role in the boundary condition.

Barrat and Bocquet[138,139] explored the influence of wetting properties on hydrodynamic boundary conditions at a fluid/solid interface. It was found that, although the fluid layering can extend 5−6 molecular diameters from the wall, slip lengths in excess of 30 molecular diameters for a contact angle of 140° can be achieved by reducing δ in eq 3, to simulate a nonwetting fluid/solid interface. In addition, a relationship between slip length and microscopic parameters of the system was developed. From this relationship, it was concluded that, for a constant δ, the slip length decreases with increased density and structuring in the first epitaxial layer. Therefore, the slip length is expected to be small in a dense fluid at high pressures. However, large slip is predicted, even in the presence of strong structuring, provided that δ is decreased, while simultaneously increasing the pressure and keeping the fluid density constant. Finally, their model predicts infinite slip at a contact angle of 180°, in conjunction with the Laplace estimate of the contact angle.

Besides the LJ parameters, slip length is a function of numerous other properties of the system. MD and direct-simulation Monte Carlo studies of slip length in dilute gases by Morris et al.[146] found that the slip length increases with Knudsen number (*Kn*), as is predicted by the Maxwell theory. An attempt to describe shear dependence of the slip length was made by Thomson and Troian,[69] who developed a general boundary condition that expressed slip length as a nonlinear function of the critical shear rate ($\dot{\gamma}_c$) as follows:

$$b = b^o\left(1 - \frac{\dot{\gamma}}{\dot{\gamma}_c}\right)^{-1/2} \tag{5}$$

where b° is the asymptotic limiting value of slip length. The behavior proposed by Thomson and Troian suggests that, close to a critical shear rate, the flow can be significantly affected far away from the wall, and that various magnitudes of slip can be expected with different substrates.

Because most practical systems do not consist of monatomic fluids and flat walls, the next logical step in slip length simulations was to study complex fluids and/or nonuniform surface composition or topology. Yang[147] used NEMD to study effects of roughness on the nanorheology and on fluid slip for Stokes flow of a simple LJ fluid through attractive and repulsive nanochannels that consisted of either two flat walls, or one flat wall and one wall with grooves. The results suggest that fluid slip increases with fluid density for repulsive walls only, but it is always suppressed by roughness due to drag resistance. The slip length at the smooth wall was determined to be unaffected by the roughness of the opposite wall. Similar to many other researchers, Yang observed epitaxial fluid layering in the vicinity of the solid wall, but he also observed that the layering could be altered by modifying the wall roughness parameters. Perhaps the most interesting result to come out of the Yang study is that the fluid flow rate through smooth nanochannels increases linearly with slip length, regardless of wall affinity.

Cao et al.[115] modeled flow of a simple LJ fluid in nanochannels whose surfaces were structured by an array of nanoscale triangular modules. It was determined that slip length is always larger for repulsive walls rather than for attractive walls; and that the slip length decreases with increasing size of the roughness for attractive walls, while increasing to a maximum and decreasing thereafter for repulsive walls. The nonmonotonic

Table 3. Summary of Findings by Molecular Dynamics Simulations about the Calculation of the Slip Length

	Fluid		Solid			
author	fluid type	number of atoms	solid type	number of atoms	variables	slip (σ_{ff})
Koplik and Banavar[153] (1989)	LJ	1536	vibrating FCC	256	T, ρ_f	56
Thompson and Robbins[145] (1990)	monatomic LJ	672	vibrating FCC	192−352	ρ_{sf}, ρ_s	−2.5 to 3.5
Morris et al.[146] (1992)	monatomic LJ or variable hard sphere	1000	not specified		Kn	0−21
Thompson and Troian[69] (1997)	monatomic LJ	1152−1728	FCC	144−576	shear rate, ϵ_{sf}, σ_{sf}, ρ_s	0−38
Barrat et al.[138, 139] (1999)	monatomic LJ	1000	fixed FCC	9000	δ, P	2−42
Galea and Attard[78] (2004)	monatomic LJ	6000	vibrating FCC		σ_{ss}	−3 to 4
Sokhan et al.[150] (2001)	monatomic LJ		LJ-TB[154] graphene, CNT		ϵ_{sf}	−0.9 to 27
Priezjev et al.[155] (2005)	monatomic LJ	30720	FCC w/ alternating slip stripes on one wall	24576 (FCC)	flow direction, ϵ_{sf}, stripe width and period	2−110
Cao et al.[115] (2006)	monatomic LJ	5200	vibrating FCC smooth or with isosceles triangular grooves	2000	isosceles side length, ϵ_{sf}	−1.92 to 23.1
Yang and Fang[156] (2005); Yang[147] (2006)	monatomic LJ		vibrating FCC, smooth or with grooves on one wall		δ, σ_{ss}/σ_{ff} ρ_f, degree of wall roughness	−3 to 8
Jabbarzadeh et al.[148] (2000)	LJ hexadecane to butane	variable	vibrating sinusoidal BCC	3 layers	fluid chain length, wall topography (amplitude, period)	up to 60% of U_{wall}
Cieplak et al.[149] (2001)	monatomic LJ, polymeric LJ/FENE		vibrating FCC	192−352	δ, T_s, ρ_f, flow type (Couette- and gravity-driven)	−3 to 20.6
Cieplak et al.[116] (2006)	LJ chains/FENE	240−1200	vibrating FCC −roughness		ρ_f, roughness types	>12
Walther et al.[152] (2004)	SPC/E water	18500	rigid CNT	320−640	CNT diameter, flow speed and orientation	−0.11 to 0.88 nm

behavior of the slip length with surface roughness size was attributed to dual counteracting effects: hydrodynamic distortion of streamlines of the liquid flow and the nanoscale lotus effect.

A study by Jabbarzadeh et al.[148] explored the effects of fluid particle size and surface topology on the slip. It was concluded that slip is larger for longer molecules, a smaller topology amplitude causes greater slip with a flat wall producing the maximum slip, and slip on the wall increases as the roughness period is increased. A study by Cieplak et al.[149] explored how the slip length varies for a monatomic LJ fluid and a fluid composed of chains of 10 LJ atoms. It was determined that the slip length is independent of the type of flow or of increases in the channel width, but it is related to the fluid organization in the vicinity of the channel walls (particularly to the density buildup in the second layer normal to the wall) as governed by the fluid/solid molecular interactions. At lower fluid densities and at repulsive wall conditions achieved by reducing δ in eq 3, the slip length is maximized. Chain molecules showed greater sensitivity in slip length behavior to variations in δ.

As in the case of contact angle simulations, graphitic systems attract much attention today. Sokhan et al.[150,151] modeled the Poiseuille flow of methane in slit carbon nanopores and in a CNT. As a result of these studies, it was concluded that, even for the strongly wetting case, both flows are characterized by a large slip length, and a slip boundary condition was proposed for smooth continuum surfaces, such that the boundary condition would be consistent with fully dynamic atomistic models, with respect to adsorption, diffusion, and fluid flow properties. Walther et al.[152] studied water flow past an array of single-walled carbon nanotubes (SWCNTs) fixed in space. Reasonable agreement was achieved with the macroscopic Stokes−Oseen solution for flow past a cylinder. The slip length was determined to be larger for a larger CNT diameter for the same flow velocity, and it was determined to increase with flow velocity for all but one cases. However, maximum slip was obtained in the case of flow parallel to the CNT.

In summary, MD methods have been rigorously validated against analytical solutions of the Stokes and Navier−Stokes equations. They form a legitimate tool for the exploration of microscopic fluid dynamics. Slip, no-slip, and locking boundary behavior has been observed. Slip length seems to be a function of a bouquet of variables, such as fluid density and molecule size, shear rate, and surface roughness.

A discrepancy between experiments and simulations exists, in regard to the order of magnitude of the slip length: simulation predictions underestimate experimental results by several orders of magnitude. The answer to this discrepancy may lie in the fluid arrangement near the solid boundary. Numerous simulation studies, as well as some experimental studies, have observed the formation of epitaxial layers in the fluid that mimic the solid structure near the solid−fluid interface (see section IV.b). Most of the researchers agree that the slip boundary behavior is closely related to, and is perhaps dominated by, these structures. Because the epitaxial fluid layers mimic the solid lattice, it is also logical to conclude that the slip length is dependent on the nature of the solid lattice next to the solid/fluid interface. Thus, consistency in the solid type between experiment and simulation is required to reconcile any differences in measured results. Finally, the fact that nonmonatomic behavior of the slip, relative to surface roughness size, has been observed suggests that the quest for a surface with maximum slip length will not be simply resolved by increasing one parameter, but instead will be determined by some favorable combination of pertinent variables.

Table 3 summarizes the MD simulations findings of slip length calculations. Note that simulations on complex surfaces are further discussed in section IV.b.

IV. Contact Angle−Slip Length: Is There a Connection?

A basic issue that arises now is to elucidate the relationship between the two characteristics of solvophobicity: contact angle and slip length. An attempt at relating contact angle to slip length

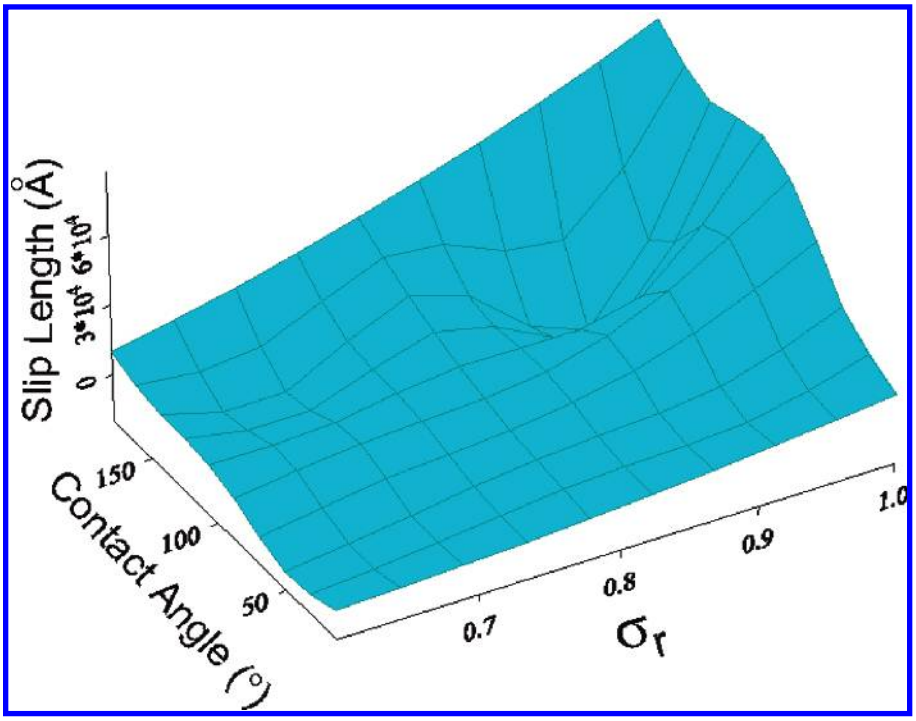

Figure 4. Three-dimensional depiction of the slip length−contact angle−relative size space at $T = 83.3$ K. (Reprinted with permission from Voronov et al.[159] Copyright 2007, Elsevier B.V. Publishers.)

was previously made by applying Blake−Tolstoi theory,[157] which justified slip in terms of the underlying molecular-kinetic mechanism and proposed that the mobility of the liquid molecules adjacent to a solid surface is dependent on the equilibrium contact angle of the liquid on the solid.[84] The resulting model showed that contact angle and slip length are not simple functions of each other, but are also functions of the fraction microcavity area within the solid, of the fluid intermolecular separation, and, most importantly, of the fluid molecular size. A limitation of the Blake−Tolstoi model is that it does not consider how the solid structure affects that of the fluid in close vicinity to the wall. In fact, the fluid structure close to the wall is detrimental to slip behavior, because of the formation of epitaxial layers. Thus, the use of a method such as MD, which would be able to account for all these limitations, would give a more-accurate picture of the physics involved (although, recently, the use of lattice Boltzmann methods, in conjunction with theory, has become a viable alternative to MD when trying to tackle this problem[158]).

IV.a. Contact Angle−Slip Length−Relative Size 3D Map. To determine if it is correct to assume that a surface deemed to be hydrophobic (or solvophobic), because of a high contact angle, will produce significant drag reduction, both EMD (for contact angles) and nonequilibrium molecular dynamics (NEMD) (for planar Couette flow) were performed by Voronov et al.,[74,159] using the MD code LAMMPS.[160] The contact angle (an indicator of wetting) and the slip length (an indicator of drag reduction) behaviors were compared to each other, as a function of nondimensional LJ parameters. The idea was that, if the contact angle and the slip length behave differently for a simple LJ model, then they would also behave differently for more-complicated systems. The authors simulated a LJ fluid (argon), and the walls confining it were chosen to resemble graphite in a hexagonal lattice arrangement.[161]

The contact angle-slip length relationship can be visualized on a three-dimensional (3D) map.[159] Figure 4 shows a slip length−contact angle−σ_r space 3D map. It was created by eliminating one of the two LJ parameters (defined in eq 4), ϵ_r, between the parametric contact angle and slip length results (because the relative size is more readily determined than ϵ_r, in most cases). Figure 4 shows that slip length does indeed increase with larger contact angles; however, the conventional belief that maximum contact angle corresponds to maximum slip length is not entirely correct, because it is possible for slip length to decrease as contact angle increases or remains constant (as one travels along the contact angle−σ_r surface).

According to the contact angle−slip length−σ_r 3D map, fluid−solid pairs with similar sizes and contact angles in the range of 90°−140° produce maximum slip. These results show that, even for a simple fluid−solid interaction model, the idea that higher contact angle will reduce friction drag is not always true. When designing supersolvophobic surfaces, one should also take into account the size of the solid atoms, relative to those of the fluid.

Figure 4 is meant to be a qualitative guide, rather than a quantitative one, for superhydrophobic surface design (unless the fluid−solid pair is a monatomic LJ fluid and a hexagonal solid lattice). Because computer modeling is becoming a mainstream tool in surface science, analagous parametrical maps should be generated for more complicated fluid−solid pairs, where the slip length and the contact angle are related as a function of other significant parameters (see section IV.c for a discussion of such parameters).

Epitaxial Layering and Its Role in Slip. Why does higher solvophobicity induce smaller slip as σ_r diminishes? The interpretation is that, for smaller σ_r, the central sites (holes) in the hexagonal lattice have a tendency to "trap" the Ar atoms, because the Ar atom seems to be smaller than the lattice carbons. The trapped Ar atoms are dragged along, as the wall translates, in the form of a structure similar to that of the solid lattice up to three atomic diameters away from the wall. The momentum transfer from the wall to argon fluid is more efficient. At larger σ_r the lattice sites no longer retain the argon atoms effectively, and the solvophobic effect takes over. An abundance of simulation studies found that the slip length is linked to the fluid organization near the solid, as governed by the fluid−

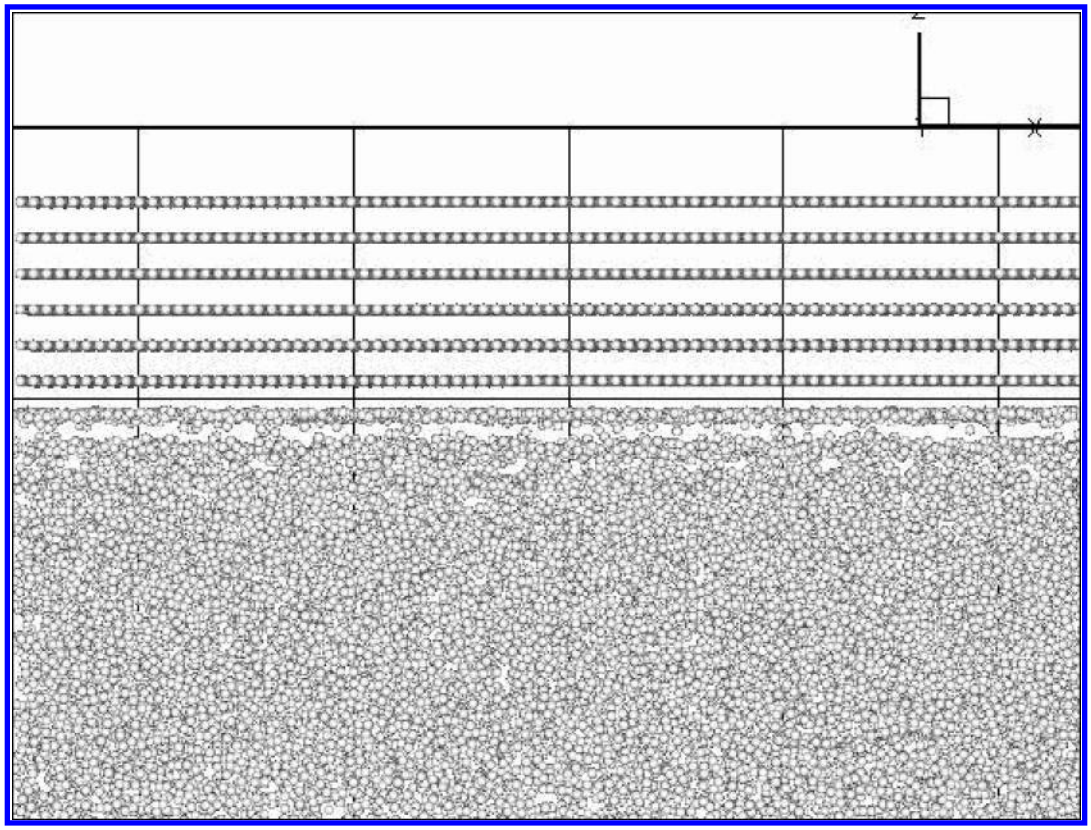

Figure 5. Fluid molecules form epitaxial layers in proximity to the wall, mimicking the solid lattice structure ($\sigma_r = 0.92$, $T = 107.82$ K, and $U_o = 0.01$ Å/fs). (Reprinted with permission from Voronov et al.[74] Copyright 2006, American Institute of Physics.)

solid molecular interactions, specifically in the first and second fluid layers normal to the wall.[145,149,162] In particular, the slip increased as the fluid density decreased in the epitaxial layers close to the wall.[145,149] On the experimental side of things, Israelachvili was able to conclude, based on SFA experiments, that solvent structuring at surfaces does not necessarily affect the liquid viscosity (a region of low viscosity near the wall is a prerequisite for apparent slip),[163] and nor does it have any significant effect on the hydrodynamic flow beyond the first layer of molecules.[164] Unfortunately, no direct experimental evidence exists today to either confirm or rebuke the connection between slip and fluid organization near the solid wall, because of limitations of the current experimental techniques. Despite this observation, epitaxial layering is worth further explanation, because it turns out to be detrimental to analysis of the slip length mechanism.

Figure 5 shows the fluid layer mimicking the solid lattice, in what is referred to as an epitaxial layer arrangement.

Epitaxial-like layering has been observed in many simulations,[115,138,139,145,147,149,155,156] as well as experimentally.[165] A fundamental framework has been laid out by Bocquet and Barrat[166] for developing the dependence of the slip length on molecular parameters based on the Green-Kubo relations. This approach allows computing of the slip length based on equilibrium calculations, thereby avoiding the problems inherent to nonequilibrium simulations, such as temperature control and high velocity gradients. Later, Priezjev and co-workers[80,155] used it to develop and verify an expression for the slip length based on the first epitaxial layer contributions to the fluid force−force correlation functions. Only the first epitaxial layer contributions were used in the derivation, because they were assumed to be the most significant, and the other epitaxial layer contributions were neglected. Although the slip length expression seems to work well for the limiting case of a pronounced first epitaxial

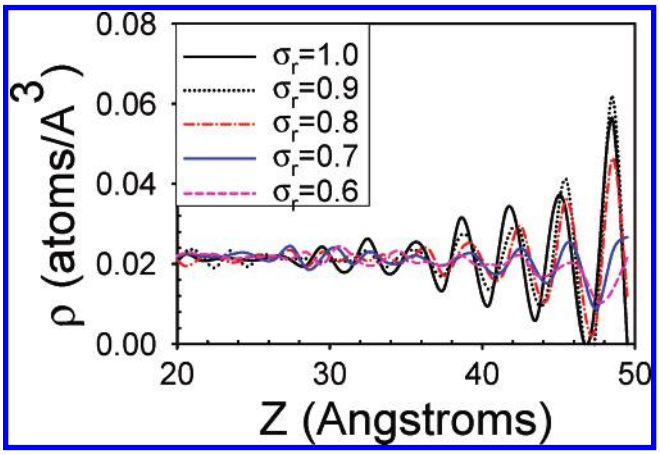

Figure 6. Density profiles in the *YZ* plane (averaged in the *X*-direction over 100 000 time steps) at $T = 83.3$ K, $\epsilon_r = 0.3$, and $U_o = 0.01$ Å/fs. (Reprinted with permission from Voronov.[48] Copyright 2006, University of Oklahoma.)

layer, it is expected that this relationship would not hold for the cases when there is not much density variation between the successive fluid layers and the contributions are comparable. Such cases have been observed to occur at low σ_r.[159]

Figure 6 has been taken from the simulations of Voronov et al.[159] The epitaxial layers are denser for high σ_r, and they decerase in density as σ_r diminishes. Another peculiar thing in this figure is that the amplitude of the density variations becomes smaller as σ_r diminishes (probably due to tighter packing). This means that, as σ_r decreases, the fluid density close to the wall becomes more uniform (its value nears that of the bulk fluid) and almost no epitaxial layers are present near the wall. The wall drags the fluid more efficiently, because no low-density regions can interrupt the momentum transfer. At large σ_r, on the other hand, the fluid density variations are much more

Table 4. Contact Angle Behavior on Flat Heterogeneous Surfaces from Simulations

reference	surface type	contact angle behavior	variable behavior
Schneemilch et al.[92]	energetic stripes	↓	↓ (pattern wavelength)
Lundgren et al.[169]	energetic stripes	maximum	at pattern wavelength commensurate to drop radius
Lundgren et al.[169]	energetic squares	↑	↓ (domain size)

Table 5. Contact Angle Behavior on Rough Surfaces (from Simulations and Calculations)

reference	surface type	contact angle behavior	variable behavior
Porcheron and Monson[39] (2006)[a]	square posts	↑ (to saturation)	↑ (post height)
Lundgren et al.[169] (2007)			
Lundgren et al..[169] (2007)	square posts	↓	↑ (post width)
Lundgren et al.[169] (2007)	square posts	↑ (to saturation), or maximum	↑ (post separation)
Cao et al.[115] (2006)	triangular grooves (isosceles)	↑ (for repulsive walls) constant (for attractive walls)	↑ (isosceles side length)

[a] Calculations based on Mean Field Density Functional Theory (MF−DFT).

pronounced, signifying the presence of epitaxial layers and also gaps (or regions of low density) between them. This interpretation differs from the Cieplak et al.[148] study, in that it relates the increase in the slip length to the gaps between the epitaxial layers and not to the layers themselves.

The epitaxial layering may also help explain the difference between large slip length on FCC solids and on graphite. The graphite lattice is two-dimensional, with a *z*-spacing of ∼3.4 Å and very low interlayer frictional properties,[167] whereas the FCC lattice is three-dimensional with the density gaps between the epitaxial layers not as depleted as in the case of the two-dimensional graphite lattices. Thus, momentum would be transferred more efficiently from the solid wall to the fluid, in the case of the FCC or any other 3D lattice. A study of the effects of gap size between the epitaxial layers on the slip length could potentially shed light on this hypothesis.

IV.b. Roughness Effects. The concept of liquid slipping past a gas trapped by solid surface imperfections, as in the Cassie regime, sparked a flurry of investigations into the influence of wall roughness. Similar to the effects caused by the solid/fluid interactions, there are also roughness effects that can cause the contact angle and the slip length to display contradictory behavior. For example, geometrical aspects, such as anisotropic patterns, roughness height, and pattern wavelength can have conflicting effects on contact angle and slip length. Recently, it has been experimentally shown that surface roughness can significantly affect drag reduction.[136] Effects of roughness on static and dynamic wetting[63] have also been investigated. In fact, roughness has been used to both increase[168] and decrease[28] wetting! Therefore, it is of interest to explore the issue of roughness further to further increase the understanding of its effects on the slip length and contact angle.

Contact Angle. Some obvious trends were observed for the contact angle on energetically patterned surfaces: the contact angle decreased as the wetting stripes became wider than the nonwetting stripes, and the contact angle increased as the fraction of hydrophobic squares that occupied a surface increased. An interesting result, from the Schneemilch et al. study,[92] is that the contact angle decreased as the wavelength of the stripes decreased. Lundgren et al.[169] did not observe this; however, instead, it was observed that the contact angle experienced a maximum at stripe widths commensurate to droplet radius and decreased at noncommensurate sizes. Contact angles were predicted well from the Cassie state equation at large wavelengths, but they deviated from the predictions at small wavelengths in the Schneemilch et al. study. Conversely, Lundgren et al.[169] observed better agreement with the Cassie state prediction at small domain sizes of energetic squares. Cieplak et al.[116] were able to maximize the static contact angle of a nanodroplet on energetic patches to 130°. Experimental findings of the contact angle on circular energetically heterogeneous islands suggest that interactions at the contact line, not the contact area, control wetting of the heterogeneous surfaces.[170] Table 4 summarizes the observed contact angle behavior on flat heterogeneous surfaces.

When topology effects were explored, the contact angle increased with post height, up to a saturation point. It decreased as the width of the square posts increased. When the separation between the posts was increased, the contact angle increased up to a point after which it either remained the same, or decreased, depending on the size of the droplet relative to the gaps (for large droplets, it remained the same; for small droplets, it decreased). Cao et al.[115] modeled the contact angles on surfaces of variable affinity for a fluid with an array of nanoscale triangular roughness. It was observed that the contact angle increases with more exaggerated roughness for repulsive walls, and remains approximately constant for attractive walls. Table 5 summarizes the contact angle behavior observed on rough surfaces.

Slip Length. An investigation by Priezjev et al.[155] of slip length on chemically patterned surfaces showed that it increases as the wavelength of the stripe pattern increases (note that the problem has been solved analytically for different geometries by Philip[171,172]). Absolute values of flow parallel to the stripes were always larger than those of the transverse flow, because no deceleration is experienced in the former case. Just as in the contact angle case, it was observed that, as the fraction of the no-slip surface coverage grows, less slip is experienced. The authors attributed the differences in slip to the fluid organization near the surface. Cieplak et al.[116] studied the effects of alternating energetic stripes on the flow of a dense and a rarified LJ chain fluid confined in a channel with patterned walls. The sharp step in the solid−fluid intermolecular interactions was observed to lead to a jump in wettability, resulting in fluid adsorption and layering on the attractive parts of the walls and a cushion of empty space near the repulsive parts of the walls, corresponding to Poiseuille flow and plug flow, respectively. The speed of the plug flow was determined to be smaller than the peak velocity of the Poiseuille flow in the dense fluid case, whereas the opposite behavior holds for the rarified fluid. The authors also considered channels patterned geometrically with homogeneous attractive wall-fluid interactions and found that

Table 6. Slip Length Behavior on Complex Surfaces from Simulations

reference	surface type	slip length behavior	variable behavior
Priezjev et al.[155] (2005)	energetic stripes	↑ (to saturation)	↑ (wavelength)
Priezjev and Troian[80] (2006)	sinusoidal roughness	↓	↑ (height/wavelength)
Jabbarzadeh et al.[148] (2000)	sinusoidal roughness	↑	↑ (wavelength)
Jabbarzadeh et al.[148] (2000)	sinusoidal roughness	↓	↑ (height)
Jabbarzadeh et al.[148] (2000)	sinusoidal roughness	↓	↑ (molecule size)
Cao et al.[115] (2006)	isosceles triangular grooves	first ↑, then ↓ (for repulsive walls) ↓ (for attractive walls)	↑ (isosceles side length)

Table 7. Slip Length and Contact Angle Behaviors on Complex Surfaces from Simulations: Differences and Similarities

different −/same +	contact angle behavior	slip length behavior	variable behavior
+/− (nonmonotonic behavior)	increases to maximum, then decreases	↑ (to saturation)	↑ (energetic stripe wavelength)
+	↑ (to saturation), or maximum	↑	↑ (roughness wavelength for slip and post separation for contact angle)
-	↑ (to saturation)	↓	↑ (roughness height)
+/− (nonmonotonic behavior)	↑ (for repulsive walls) constant (for attractive walls)	first ↑, then ↓ (for repulsive walls) ↓ (for attractive walls)	↑ (isosceles side length)

they behaved much like uniform width channels, as opposed to similar geometrically patterned channels but with uniformly repulsive walls that produced large slip.[173]

In a later study, Priezjev and Troian[80] studied the influence of sinusoidal surface roughness on the slip behavior of a Newtonian liquid in steady planar shear, using three different approaches: Stokes flow calculations, MD simulations, and a statistical mechanical model for the friction coefficient between a corrugated wall and the first liquid layer. In all approaches, the slip length decreased monotonically as the amplitude values increased and the pattern wavelength values decreased.

Jabbarzadeh et al.[148] investigated the case of fluid molecules that are comparable in size to the surface roughness. It was found that larger wall amplitude (height) and period (wavelength) of the sinusoidal roughness decreased and increased the slip, respectively. This is in agreement with Priezjev et al.[80,155] In addition, it was observed that larger molecule size decreases slip, because of tangling of the molecules in the roughness gaps. Cao et al.[115] observed nonmonatomic behavior of slip length with surface roughness size. The slip length decreased as the size of the roughness for attractive walls increased, while it increased to a maximum and decreased thereafter for repulsive walls. Table 6 summarizes the observed slip length behavior on energetically and topographically heterogeneous surfaces.

One could note that Jabbarzadeh et al.[148] did not explore the case of fluid molecules smaller than the surface roughness: this is a condition that is most common in superhydrophobic design. As described in section I, natural and artificial roughness is generally on the micrometer scale, while most of fluids that are not polymers have molecules on the scale of angstroms. The effects of molecule size on the contact angle have not been explored, although Lundgren et al.[169] came close, by considering the size of the droplet relative to the roughness size.

Table 7 is a summary of differences and similarities observed between the contact angle and the slip length. Although it is difficult to combine results from different studies, on different types of surface heterogeneity and fluids, it can be concluded that slip length and contact angle are related to each other, but situations do arise when surface heterogeneity can cause them to display opposite trends.

Roughness and Transition to the Wenzel State. In the simplest case of a completely flat surface, the condition is either that of slip, partial slip, or no slip, depending on the fluid−solid interactions (although it was argued that the slipping boundary condition is the correct choice for low-density gas flow past a smooth surface[174]). Two distinct mechanisms for slip have been proposed: that due to localized defects in the fluid layer near the wall and that due to shear moving large domains of molecules concurrently.[175] After the wall becomes rough, the irregularities in the wall geometry present obstructions for the fluid flow and dissipate the fluid's energy viscously by deforming the fluid's velocity field. In this regime (called the Wenzel regime; see section I.a), there are two possibilities. First, when the solid is attractive to the fluid, the viscous dissipation of energy complements the attraction and reduces the slip length. Second, when the wall is repulsive, the fluid−solid surface area is increased, because of the presence of roughness, and the repulsion of the fluid counteracts the dissipation via deformation of the fluid velocity field. The slip length, in this case, may be increased or decreased, depending on which one of the competing effects is dominant.

For periodic wall roughness, it was determined that the slip length decreases monotonically with the product of the amplitude and the wave number of the sinusoidal roughness.[80] According to some mathematical predictions (for flat plates[176] and flow past a cylinder[177]), there is a limiting value of R (relative to D for flow about objects) at which the energy of the fluid is dissipated so much that even if the boundary condition at the solid/fluid interface is that of total slip, the net effect of roughness is that a no-slip boundary condition would be observed macroscopically.

Roughness and Transition to the Cassie State. As the roughness becomes substantial enough to provide a gap between the liquid and the solid, gas may be entrapped in the created voids. It has been experimentally verified that slip increases proportionally with the roughness length scale R (where the proportionality constant is on the order of 0.1−0.2 and is weakly dependent on the fraction of liquid−solid contact area), which is also a trend predicted by theory. In other words, for large roughness scales, the liquid will seep through into the voids and the Cassie state will collapse to the Wenzel state[39] (see section I.a for a discussion of the stability limits).

Superhydrophobicity due to gas entrapment by grooved roughness in a microchannel with a rectangular cross section

was proposed to be affected by two counteracting effects, both of which are caused by the liquid surface curving and bowing into the roughness gaps.[42] The first effect is the due to the change in cross-sectional area of the flow passage, which, in turn, causes a change in the flow rate of the fluid and, thus, in the slip length. The second effect is the change in velocity field of the fluid—when the interface bows into the groove, a residual nonzero shear stress is introduced below the level of the undisturbed surface. The relative degree of these two effects, in principle, can be controlled by the means of the magnitude of the pressure difference between the liquid-filled channel and the trapped gas. The magnitude of this effect was quantified by a dimensionless ratio: $H/(4\pi)[(P_{channel} - P_{gas})]/\gamma$, where H is the length of a fundamental cell, which is periodically repeated. It was found that greatest superhydrophobicity was exhibited when the grooves were aligned with the flow.

The idealized case of the Cassie state is that of a thin layer of gas (usually taken to be air) separating the liquid and the solid phases, with no contact between the two. It has been proposed that, for this situation and in the limit of Stokes flow, the gas layer is a continuum that sticks to the solid wall. The slip length for Couette flow then can be expressed as[178]

$$b_{continuum} = \frac{\mu_{liq}}{\mu_{air}}\left(\frac{h^2}{2D} + h\right) \tag{6}$$

where h is the air layer thickness. Dependence on the plate separation makes sense, because, at high plate separation, the dependence is lost as the D-dependent term drops out. Interestingly, as D approaches zero, the slip length approaches infinity. This seems counterintuitive, because of the fact that microchannels and nanochannels require large pressure drops to cause liquid to flow through them. However, this is also what is predicted by the Maxwell theory for low-density gases.[146] Dependence on the gas layer thickness is also peculiar, although in the large thickness limit, the equation does not make too much sense.

For rarefied gas conditions (because the nanobubbles are not a continuous layer as is observed from the experiment), the no-slip boundary condition at the air/solid interface is replaced with an appropriate boundary condition from kinetic theory, and the slip length is now expressed as

$$b_{rarefied} = \frac{1}{2D}\left(\frac{\mu_{liq}}{\mu_{air}}\right)(h^2 + 2(\in + D)h + 2\in D) \tag{7}$$

where $\in = [(2 - \sigma)/\sigma]^{2/3}\lambda$, and σ is the accommodation coefficient. However, the rarified gas derivation overestimates the slip length, and, instead, a cumulative slip length with an adjustable parameter, f, which represents the surface fraction covered by gas is used:

$$b_{cumulative} = \frac{2f\mu_{liq}[(h^2/2) + (\in + h)D + \in h]}{\mu_{air}(2 - f)D} \tag{8}$$

Energetic Roughness and the Slip Length. Analytical and numerical solutions have been developed for flows past energetically patterned surfaces by Philip[171,172] for different geometries. A Stokes flow solution for pressure driven flow in a circular pipe with an energetically periodically striped slip-no slip surface, was developed and compared to experiments by Lauga and Stone.[72] For consistency, we use the subscript "e" to represent the energetic roughness scale, R_e.

IV.c. Dimensional Analysis. In a situation when there is no governing differential equation that clearly applies, dimensional analysis may be used as a more-general approach to addressing the problem. Applying the Buckingham Pi theorem,[179] one can combine individual variables into dimensionless π groups, which are fewer in number than the original variables. It involves, initially, the listing of variables significant to a problem and then combining them into dimensionless groups. Below, we do just that for the slip length and the contact angle.

What Affects Slip Length? Length Scales. It quickly becomes apparent from the plethora of slip studies that slip length is a phenomenon that is rich in complexity. Because of its small scale (comparable to the molecular size) and the geometric characteristics of the wetted surface, the continuum approach cannot be used to address the slip problem (although an approach wettability within the continuum framework that is based on interface formation theory has been proposed[180]). For simple flows of a dilute hard-sphere gas, the slip length has been related to the viscous Kn number in accordance with the Maxwell theory.[146] In more practical situations, however, more-complicated fluids and flow geometries arise. In fact, three distinct scales deserve consideration when considering flow near a solid surface:[148,176]

(1) D, which represents the characteristic scale of the geometry that confines the fluid

(2) R, which represents the scale that characterizes the roughness affecting the flow (although this scale usually requires more than one representation, depending on the symmetry of the roughness), and

(3) L, which represents the molecular scale of the fluid molecules.

For most cases, $D \gg R \gg L$, although for long-chain molecules, R can be on the order of L, and for microfluidics applications, D can also be small enough to affect the flow. Surface heterogeneity (for example, surface impurities such as energetic stripes or patches) is regarded as energetic roughness, with size scales similar to that of geometric roughness. As with any fluid flow, the problem must also be dependent on the properties of the fluid itself, such as its density and viscosity. However, for the realistic case of the Cassie state, another degree of complexity is added by exposure of the main fluid to another fluid (typically air), which is trapped by the surface roughness or is present in the form of nanobubbles on the solid surface (it has even been suggested that the nanobubbles can pull dissolved gases out of solution).[44] Finally, the slip length is not an equilibrium property and, thus, is dependent on some driving force that moves the fluid: shear rate for Couette flow or pressure drop for Poiseuille flow.

What Affects Slip Length? Roughness Effects. Slip length is dependent on the solid substrate geometric and/or energetic roughness, as discussed in detail in Section IV.b.

What Affects Slip Length? Fluid Viscosity Effects. For the limiting case of fluid floating on an air layer (neglecting fluid−solid contact with the surface roughness), it has been suggested that the slip length follows the following relationship:[75]

$$b = h\left(\frac{\mu_{liq}}{\mu_{air}} - 1\right) \tag{9}$$

where h the air layer thickness. It has also been experimentally verified that the slip length is proportional to the viscosity of the test liquid.[134] The result that the slip length is proportional to viscosity is also obtained mathematically,[175] and it is

consistent with the previous discussion of the Cassie state in section IV.b.

Despite the ease with which fluid viscosity can be measured in an experiment, in a MD simulation, the bulk viscosity is not readily available. Fortunately, it is dictated by the fluid−fluid interaction parameters. Thus, hereafter in this paper, viscosity effects are presumed to be implicit in the specified LJ parameters.

What Affects Slip Length? Density Effects and Epitaxial Layers at the Solid/Liquid Interface. Larger wall density produces larger slip and denser epitaxial layering, with continuum walls corresponding to the largest slip. Slip increases with smaller ϵ_r, but larger ϵ_r produces denser epitaxial layers and, yet, the slip is decreased.

Slip is a function of the epitaxial layers, which, in turn, is dependent on the temperature, fluid density, solid−fluid interactions, and geometric structure of the solid. It was found that slip length is inversely proportional to the density of the first layer, and the Green−Kubo approach was used to derive an analytical expression for the slip length, in terms of equilibrium properties of the fluid and characteristics of the first epitaxial layer.[138]

What Affects Slip Length? Temperature Effects. Slip length was not observed to vary with temperature significantly,[74] with the exception of a jumplike change in the *apparent* slip length at the prewetting transition at which the formation of a film of gas or phase-separated ''lubricant'' with lower viscosity occurs between the fluid and the solid wall.[181]

In MD simulations, thermal vibration of an FCC wall used did not produce a significant difference on the slip length.[145] A weak relationship is expected to exist, however, because the vibrations reduce the ordering of the layers and the slip length is increased.

The Force Driving The Flow. For Couette flow, the driving force is the wall velocity, which can be related to the shear rate. In the case of Poiseuille flow, it can be represented by either the maximum velocity or the average velocity of the fluid profile, either of which can be related to the pressure difference driving the flow. A general nonlinear relationship between the amount of slip and the local shear rate at a solid surface was presented, based on MD simulations of Couette flow of Newtonian liquids.[69] The boundary condition is controlled by the extent to which the liquid "feels" corrugations in the surface energy of the solid (because of the present case to the atomic close-packing). As common sense would dictate, the higher the driving force, the larger the slip length, although leveling off of the slip length has been observed at high forcing.[175]

Dimensional Analysis of Slip Length. The Buckingham π theorem for the case of slip of a monatomic LJ fluid on a smooth solid, taking into account all of the parameters previously discussed, allows one to express the reduced slip length in terms of the dimensionless π_1-group as follows:

$$\frac{b}{\sigma_{sf}} = f\left(\pi_1 = \frac{U_o}{\sigma_{sf}}\sqrt{\frac{\rho_f \sigma_{sf}^{\ 5}}{\epsilon_{sf}}}, \pi_2 = \frac{\rho_w}{\rho_f}, \pi_3 = \frac{D}{\sigma_{sf}}, \pi_4 = \frac{R}{\sigma_{sf}}, \pi_5 = \frac{R_e}{\sigma_{sf}}, \pi_6 = \frac{L}{\sigma_{sf}}\right) \quad (10)$$

The π_1-group seems to be very convenient for this simplified model, and we will focus the remainder of the discussion on it. Its square root term is reminiscent of the relaxation time of an LJ fluid, $\tau = (\{m_f \sigma_{ff}^2\}/\epsilon_{ff})^{1/2}$, with the only difference being that solid−fluid interaction parameters are used instead of fluid−fluid. In essence, the π_1-group can be viewed as a dimensionless velocity, reduced by the solid−fluid length scale and a relaxation time. The velocity U_o in this group of dimensional analysis represents the force driving the flow. Although the grouping of variables in a dimensional analysis procedure is not unique for more-complex systems, intuition dictates that the next π-group would have to represent the ratio of solid−fluid densities, to address the effect of the difference in their magnitudes independently. Similarly, the effect of the solid atom diameter, relative to that of the fluid atoms, deserves a π-group of its own. Alternatively, it could be represented in terms of the lattice constant and the fluid diameter. If the lattice of the solid is not cubic in nature, the length scale of the solid could no longer be represented with one lattice constant, and the use of solid density would not be acceptable due to lack of the cubic symmetry. In that case, some combination of the parameters that describe the solid structure would have to be used, such as several different lattice constants. Both the geometric and the energetic roughness scales would also need to be represented by independent π-groups in the dimensional analysis via one or more pertinent lengths (depending on if the roughness patterns were isotropic or not in one or more dimensions). Finally, the fluid molecule length scale would also have to be complimented by some other geometric characteristics of the molecule, in the case of a polyatomic fluid. It also would have to be included in the dimensional analysis. Temperature does not appear in the analysis, because it is assumed that slip length is not affected by it.[181] Considering the number of possible dimensionless parameters that can be formed, further verification of the π_{2-6}-groups, using additional simulation data, is needed.

Interestingly, note that the square root dependence on the ratio of the strength of the liquid−liquid to liquid−solid interactions, as in the π_1-group, was also obtained from the Frenkel−Kontorova equation approach.[175] In this work, we explore the relationship between the dependent dimensionless slip length and the most important independent variable—the dimensionless driving force—while leaving the dependencies on the other π-groups for future investigations.

To elucidate the relationship between the dimensionless slip length and the π_1-group, we plotted data from Voronov et al.[159] in Figure 7. If the dimensionless analysis is, in fact, correct and the π_1-group carries a physical meaning, the dimensionless slip length data should collapse on a single curve, signifying a relationship to the π_1-group. It can be observed that (i) there is indeed a relationship between the two, and (ii) it is more or less linear, with more spread at higher values of π_1, most likely due to less-accurate slip length readings. From the inset of Figure 7, it can also be observed that some deviation from linearity is observed at low π_1-group values. The data tends toward the origin, as it should, because the slip length must be zero in the limit of $\pi_1 = 0$, instead of some negative number. The physical meaning of the origin is that it corresponds to either zero shear rate, or to an infinitely attractive surface, or to fluid diameter much larger than that of the solid. Analogously, it is expected that deviation from linearity will occur at some high values of the π_1-group, because the slip length cannot increase to infinity. The fact that the dimensionless slip length data follows a relationship that makes physical sense verifies the correctness of the choice for the combination of variables that comprise the π_1-group.

Alternative approaches to quantify the slip length in terms of dimensionless groups have also been devised by other researchers. In a recent study, Li and Xu[182] suggested a new criterion number for the boundary conditions at the solid/liquid

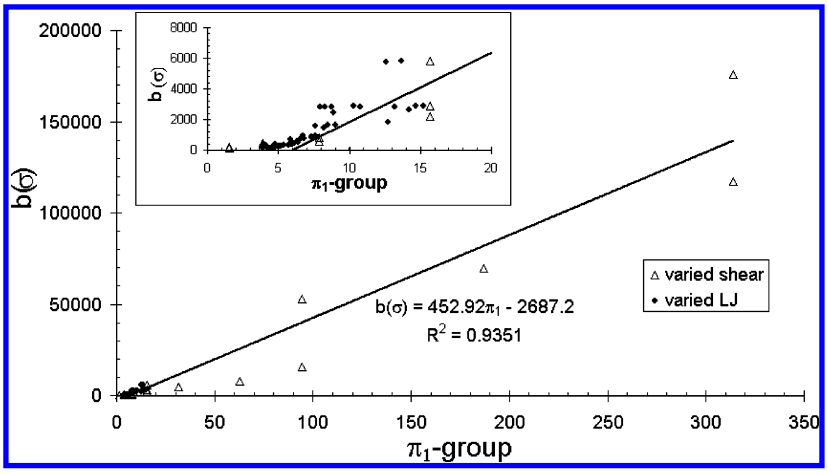

Figure 7. Dimensionless slip length versus the π_1-group for varied shear rate (triangles) and varied LJ parameters (squares). Data are taken from Voronov et al.[159] A range of wall velocities for Couette flow is explored between $U_o = 0.001$ A/fs and 0.2 A/fs. Solid line is a linear fit through the data. Inset shows an enlargement of the area near the origin.

interface in nanoscale. The slip length was determined to be a function of $(\epsilon_{sf}/\epsilon_{ff})^{-0.07}$ and of λ^2, where $\lambda = (\sigma_{sf}/\sigma_{ff})(\rho_s/\rho_f)^{1/3}$. Analytically, and from simulation, the minimal reduced slip length was predicted to occur at the critical value $\lambda_c = 0.757$.

Dimensionless Analysis for the Contact Angle. Significantly less work has been put into the exploration of the molecular mechanism underlying the contact angle, compared to that of the slip length. From Young's Law presented in section I.b, it is known that the contact angle can be described in terms of three parameters, some of which are not easily measured: γ_{sv}, γ_{sl}, and γ_{lv}. In a contact angle simulation, fixing the fluid density and temperature, the LJ parameters for all interactions and the solid positions are sufficient to specify the problem.

Similar to the slip length, the contact angle has been observed to be a function of the LJ parameters, but the dependency on σ is opposite for the two (as was discussed previously in section IV.a). The contact angle varies significantly with temperature, in contrast to the slip length, which shows no substantial variation with this parameter.[74] The temperature dependence of the contact angle seems to be a nonmonotonic one:[183] proportional for some fluids (such as the monatomic LJ fluid[86]) and inversely proportional for other fluid types.[102]

Crystalline layers have been observed in contact angle simulations, similar to epitaxial layers observed in slip studies, which actually rotated to position themselves, relative to hexagonal energetic patches on the heterogeneous solid surface, in such a way as to minimize the total energy.[93] However, as of yet, the epitaxial layers are not known to have any part in the determination of the contact angle. This is distinctive from the slip length, where the epitaxial layering seems to have a major role in the slip mechanism. It makes sense that the contact angle is not affected by the layers, because, unlike the slip length, the contact angle is not a boundary-based phenomenon. The findings of Janecek and Netz[114] support this claim, because epitaxial layers mimic the substrate structure and the contact angle was observed to be independent of the substrate structure.

Another big difference between the contact angle and the slip length is that the system geometry, and molecule size, do not have a significant role, so long as no roughness is present or no macromolecules are involved. The role that the substrate has in the contact angle is fundamentally different from the way it affects the slip length. Only the magnitude of the fluid−solid interaction forces arising from the presence of the substrate has a role, because the presence of epitaxial layers does not encourage or impede the formation of the droplet.

Therefore, ignoring impurity effects and roughness, and ruling out the effects of the solid roughness near the solid/fluid interface on the contact angle, it can be presumed that the contact angle is a function of the form $f(\epsilon_{sf}, \sigma_{sf}, \rho_f, T)$ or, equivalently, of the form $f(\epsilon_{sf}, \sigma_{sf}, \rho_f, m_f U_f^2)$, because temperature is related to the average kinetic energy via the Boltzmann constant.

Applying the Buckingham π theorem, we obtain

$$\theta = f\left(\pi_1 = \frac{\epsilon_{sf}}{\epsilon_{ff}}\frac{T}{\epsilon_{ff}/k_B}\frac{\sigma_{sf}^3}{m_f}\rho_f, \pi_2 = \frac{\rho_w}{\rho_f}, \pi_3 = \frac{D}{\sigma_{sf}}, \pi_4 = \frac{R}{\sigma_{sf}}, \pi_5 = \frac{R_e}{\sigma_{sf}}, \pi_6 = \frac{L}{\sigma_{sf}}\right) \quad (11)$$

The first π-group is essentially $\epsilon_r T^* \sigma_r^3 \rho_f^*$ and is reminiscent of the Hamaker constant.[86] It is the only dimensionless combination of variables that properly describes the behavior of a monatomic LJ fluid near a flat wall. Considering the number of parameters for more-complicated systems, there is no way to be certain as to the correctness of the remaining π-groups without additional data. However, intuition dictates that, as in the case with the slip length, the π-groups should represent the ratio of solid-fluid densities, the ratio of the solid atoms scale over the fluid atom scale, dimensionless geometric and energetic solid roughness scales, and fluid molecular structure characteristics, to account for each of these effects independently. In the case of a non-cubic solid lattice, non-isotropic roughness, or polyatomic fluid molecules, the respective π-groups would have to be supplemented by additional length scales to account for the additional degrees of freedom. The nature of these groups is only speculation, and a detailed analysis of their behavior is outside the scope of the present review. We focus here on the first group, which is formed by quantities that are used as simulation parameters.

To elucidate the relationship between the contact angle and the π_1-group, we plot data from Voronov et al.[159] in Figure 8. The contact angle−π_1-group relationship seems to be a power law; thus, the π_1-group provides a convenient way to correlate the contact angle data. The fact that the contact angle data collapse on a single curve verifies the correctness of the π_1-group (no other dimensionless combination of the variables achieves this). At low values of the π_1-group, the relative energy parameter (ϵ_r), the temperature (T), or the relative atom size (σ_r) is small and the contact angle approaches 180°, as expected. The minimum contact angle occurs at high values of π_1-group.

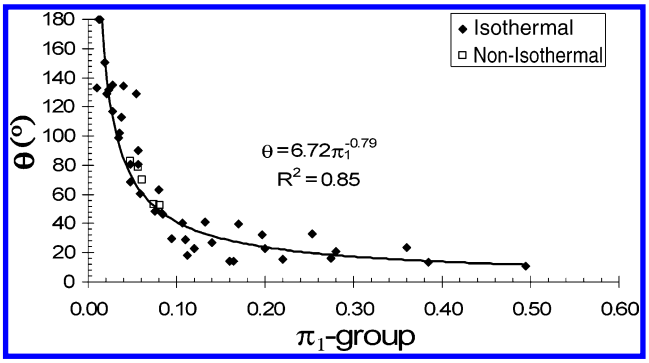

Figure 8. Contact angle versus the π_1-group for varied LJ parameters at $T = 83.3$ K (filled data points) and varied temperature data at $\epsilon_r = 0.3$ and $\sigma_r = 0.7$ (empty data points). Solid line is a power fit through the data. Data are taken from Voronov et al.[159]

Both the non-isothermal and isothermal data collapse onto a single curve, signifying the validity of the developed dimensionless group. Importantly, note, however, that this trend is for a graphitic substrate, and although a relationship should still exist between the contact angle and the dimensionless group for a different type of lattice, its nature may be different.

IV.d. Contact Angle and Slip Length: The Unification. It can be inferred from algebraic rearrangement of eqs 10 and 11 that if we conveniently eliminate ϵ_{sf} (because it is practically impossible to measure experimentally) from the two π_1-groups, the following analytical relationship arises:

$$\pi_{1,\mathrm{slip}} = \left[\frac{\rho_f^{\,2}\sigma_{sf}^{\,6}U_o^{\,2}T^*}{m_f\pi_{1,\mathrm{CA}}\epsilon_{ff}}\right]^{1/2} = \rho_f U_0\left[\frac{(\sigma_{ff}\sigma_{ss})^3 k_B T}{m_f\pi_{1,\mathrm{CA}}\epsilon_{ff}^{\,2}}\right]^{1/2} \quad (12)$$

This relationship should hold for any monatomic LJ fluid paired with a solid lattice without any macroscopic roughness or energetic heterogeneity. The beauty of this relationship comes from the fact that, although it is derived from MD simulations, all except for one variable are practically measurable quantities. The only exception is the fluid−fluid interaction LJ energy (ϵ_{ff}). Fortunately, fluid−fluid LJ parameters can be obtained through analysis of the experimental data for the second virial coefficients, the viscosity, and the Joule−Thompson self-diffusion coefficients. Although rough estimates can be obtained from the constants characteristic of the critical melting (or boiling) points, more-precise methods for determining the LJ parameters have been proposed and their values for some simple gases have been tabulated.[184]

When the fluid−solid pair has been fixed, the π-groups in eq 12 can be replaced by actual empirical relationships for the contact angle and the slip length. In the case of graphite and argon, we can use the relationships from Figures 7 and 8 to produce a relationship that unifies the static contact angle and the reduced slip length, in its final form:

$$b = 134.75\theta^{0.63}\rho_f U_0\left[\frac{(\sigma_{ff}\sigma_{ss})^3 k_B T}{m_f\epsilon_{ff}^{\,2}}\right]^{1/2} - 2687.2 \quad (13)$$

Equation 13 shows that the slip length will vary from one fluid−solid pair to another, even if the contact angle is the same for both of them. Thus, the assumption that a high contact angle maximizes the slip of a fluid past a surface is relaxed.

V. Summary and Conclusions

This work provides an overview of the hydrophobicity phenomenon and of attempts to manufacture hydrophobic surfaces to achieve friction−drag reduction. The basic surface science concepts involved, a historical perspective, and current developments in the experimental and in the modeling approaches to hydrophobicity have been provided. A fundamental question concerning the legitimacy of using the contact angle (an easily measurable "hydrophobicity gauge") as a precursor to slip (or friction drag reduction) when evaluating hydrophobic surfaces is addressed via molecular simulation and by theoretical analysis.

Slip is the ultimate indicator of friction−drag reduction, but it is extremely difficult to measure experimentally, because of its microscopic nature. Techniques tracing the fluid flow near a boundary and techniques based on force or displacement measurements are among the most common methods currently used. There is much criticism and doubt in regard to the validity of the results obtained by such experiments, because of technological limitations, and the very existence of slip on wetting surfaces is still being debated. However, its existence on hydrophobic surfaces has been more or less accepted. Moreover, both the contact angle and the slip length have been elusive theoretically, when dealing with realistic solid substrates that have geometric roughness on their surface. Given these hurdles, the scientific community has turned to computational experiments in its search for answers.

Although modeling interactions of complex fluids and solids remains a challenging subject to this day, the swiftly paced progress of computational science renders molecular dynamics (MD) simulations a preferred tool for exploring the nature of such physical phenomena. When a simple case of a Lennard-Jones fluid (e.g., argon) on graphite is studied using MD, the contact angle and slip length follow the same trends only within a particular range of conditions, but they can actually be inverse to each other under other conditions (although the contact angle increases with lower σ_r, friction drag is actually reduced at higher σ_r). The main difference in behavior between the contact angle and the slip length is attributed to epitaxial layering of the fluid near the solid surface. Because the slip length follows the opposite trend than the contact angle for different solid: fluid size ratios, care must be taken when designing slip surfaces by taking into account the structure and properties of materials.

To achieve further comprehension of the mechanisms behind slip length and contact angle, dimensional analysis is used to develop sets of dimensionless parameters from the independent variables given at hand. Independent scaling of the slip length and contact angle with their respective fundamental dimensionless groups is elucidated for the two phenomena in the context of simple systems. Scaling of slip length with the contact angle is inferred in the form of a semiempirical relationship for the argon−graphite system. The relationships obtained via the dimensionless analysis approach pave a way to the unification of a plethora of intricate factors that are involved in determining the degree of hydrophobicity for more-practical systems. The dimensional analysis approach lays the foundation for exploration of the relationship between the contact angle and the slip length theoretically. Despite this progress, much more work remains to be done in this area to account for geometric roughness, energetic heterogeneity, and polyatomic molecular structure.

However, much room is left for further improvement and future investigations of hydrophobicity. First, experimental techniques should be improved to capture the microscopic nature of slip more accurately (most importantly, a consensus of magnitude should be achieved). Because friction−drag reduction is the ultimate goal of these studies, larger hydrophobic surface samples should be created and experiments such as pressure

drop in a pipe should be performed. Second, discrepancies in the literature between experimental and computational measurements of the slip length, although they can be possibly attributed to substrate structure effects on the epitaxial layering, must be further reconciled by consistently making both types of measurements on the same type of solid substrate. To accomplish this, both experimentalists and modelers should examine effects of the two-dimensional (2D) solid substrate lattices on the slip length, as opposed to three-dimensional (3D) ones (something that has rarely been done before), and effects on the slip length of the density gaps that are formed when the fluid near the interface mimics the solid substrate structure. Finally, improved theoretical understanding of both the slip length and the contact angle is needed to be able to account for geometric and energetic roughness, for the solid substrate structure, for molecular complexity of the fluid in question (such as water), and for the effects of solid and fluid impurities.

Slip length experiments are still in their infantile stage; therefore, the contact angle measurements for gauging superhydrophobic surfaces are not going to go away in the near future. Therefore, perhaps the most important challenge to the scientific community is to establish a well-defined correlation between the slip length and the contact angle. To accomplish this, further exploration into the subject is needed. Perhaps the key issue that must be resolved is the opposite behavior of the slip length and contact angle relative to the solid:fluid size ratio. As available computing power grows, large-scale MD should be performed for more-complicated fluid−solid pairs and the relationships between them should be clarified, as well as validated experimentally. Ideally, libraries of such data could be collected to enable the development of a robust theory.

In summary, using the contact angle as a measure of hydrophobicity, and sometimes as fluid slip gauge, can be misleading when it comes to designing superhydrophobic friction-reducing surfaces. As can be seen from the increasing frequency of publications on both subjects, the exploration of contact angle and slip length on both simple and complex surfaces is a dynamic field of research with many potential applications in friction−drag reduction. Acquiring insight into these subjects would be enormously beneficial to future optimization of surface patterning with drag reduction in mind.

Nomenclature

b = slip length
D = length scale characterizing the flow geometry
f = surface fraction covered by gas
k_B = Boltzmann constant
h = air layer thickness, from ref 178
H = dimensional cell width, from ref 42
m = mass
Kn = Knudsen number
L = depth of flow field or molecular dimension
P = pressure
R = lateral radius of the droplet or scale characterizing the roughness affecting the flow
r = distance between the particles
T = temperature
T^* = reduced temperature in LJ units; $T^* = k_BT/\epsilon$
U = velocity
X = head group
x = direction of flow
z = direction normal to the surface

Greek Characters

γ = surface tension
$\dot{\gamma}$ = shear rate
δ = constant artificially introduced into the Lennard-Jones potential to vary the strength of attraction
∂ = constant artificially introduced into the Lennard-Jones potential to vary the strength of repulsion
ϵ = Lennard-Jones potential well depth
λ = mean free path (kinetic theory) or criterion number from ref 182
μ = fluid viscosity
π_i = dimensionless groups, where i is the number of the group
θ = contact angle
ρ = density
ρ^* = reduced density in LJ units = $\rho\sigma^3/m$
σ = Lennard-Jones particle size or accommodation coefficient (kinetic theory), from ref 178
τ = line tension or relaxation time
Φ = potential energy

Subscripts

0 = at/of the graphite wall
∞ = macroscopic quantity
CA = contact angle
CO = carbon−oxygen interaction
c = critical
e = energetic
f = fluid
int = interface
i,j = species or surface type
liq = liquid
LV = liquid vapor
r = relative
SLIP = slip length
SL = solid liquid
SV = solid vapor
s = solid
w = wall
x = streamwise direction

Superscripts

′ = extrapolated distance
o = asymptotic limiting value
* = dimensionless

Accent

· = derivative, with respect to time

Acknowledgment

We would like to acknowledge the support of the Office of Naval Research (under Grant No. N00014-03-1-0684, administered by Dr. R. N. Joslin). Computations were performed with the help of Henry Neeman at the OU Supercomputing Center for Education & Research (OSCER).

Literature Cited

(1) Eijkel, J. Liquid slip in micro- and nanofluidics: recent research and its possible implications. *Lab Chip* **2007**, *7* (3), 299.

(2) Whitesides, G. M.; Stroock, A. D. Flexible methods for microfluidics. *Phys. Today* **2001**, *54* (6), 42.

(3) Min, T. G.; Kim, J. Effects of hydrophobic surface on skin-friction drag. *Phys. Fluids* **2004**, *16* (7), L55.

(4) Ou, J.; Perot, B.; Rothstein, J. P. Laminar drag reduction in microchannels using ultrahydrophobic surfaces. *Phys. Fluids* **2004**, *16* (12), 4635.

(5) Ou, J; Rothstein, J. P. Direct velocity measurements of the flow past drag-reducing ultrahydrophobic surfaces. *Phys. Fluids* **2005**, *17* (10), 103606.

(6) Fukagata, K; Kasagi, N; Koumoutsakos, P. A theoretical prediction of friction drag reduction in turbulent flow by superhydrophobic surfaces. *Phys. Fluids* **2006**, *18* (5), 051703.

(7) Choi, C.-H.; Ulmanella, U.; Kim, J.; Ho, C.-M.; Kim, C.-J. Effective slip and friction reduction in nanograted superhydrophobic microchannels. *Phys. Fluids* **2006**, *18* (8), 087105.

(8) Schnell, E. Slippage of Water Over Nonwettable Surfaces. *J. Appl. Phys.* **1956**, *27* (10), 1149.

(9) Li, H. J.; Wang, X. B.; Song, Y. L.; Liu, Y. Q.; Li, Q. S.; Jiang, L.; Zhu, D. Super-"amphiphobic" aligned carbon nanotube films. *Angew. Chem., Int. Ed.* **2001**, *40* (9), 1743.

(10) Extrand, C. W. Designing for optimum liquid repellency. *Langmuir* **2006**, *22* (4), 1711.

(11) Extrand, C. W. Criteria for ultralyophobic surfaces. *Langmuir* **2004**, *20* (12), 5013.

(12) Carbone, G.; Mangialardi, L. Hydrophobic properties of a wavy rough substrate. *Eur. Phys J., E* **2005**, *16* (1), 67.

(13) Gao, X. F.; Jiang, L. Water-repellent legs of water striders. *Nature* **2004**, *432* (7013), 36.

(14) Feng, L.; Li, S. H.; Li, Y. S.; Li, H.; Zhang, L.; Zhai, J.; Song, Y.; Liu, B.; Jiang, L; Zhu, D. Super-hydrophobic surfaces: From natural to artificial. *Adv. Mater.* **2002**, *14* (24), 1857.

(15) Oner, D.; McCarthy, T. J. Ultrahydrophobic surfaces. Effects of topography length scales on wettability. *Langmuir* **2000**, *16* (20), 7777.

(16) Yabu, H.; Shimomura, M. Simple fabrication of micro lens arrays. *Langmuir* **2005**, *21* (5), 1709.

(17) Ma, M. L.; Mao, Y.; Gupta, M.; Gleason, K. K.; Rutledge, G. C. Superhydrophobic fabrics produced by electrospinning and chemical vapor deposition. *Macromolecules* **2005**, *38* (23), 9742.

(18) Balasubramanian, A. K.; Miller, A. C.; Rediniotis, O. K. Microstructured hydrophobic skin for hydrodynamic drag reduction. *AIAA J.* **2004**, *42* (2), 411.

(19) Onda, T.; Shibuichi, S.; Satoh, N.; Tsujii, K. Super-water-repellent fractal surfaces. *Langmuir* **1996**, *12* (9), 2125.

(20) Sun, M. H.; Luo, C. X.; Xu, L. P.; Ji, H.; Ouyang, Q.; Yu, D.; Chen, Y. Artificial lotus leaf by nanocasting. *Langmuir* **2005**, *21* (19), 8978.

(21) Liu, B.; He, Y. N.; Fan, Y.; Wang, X. G. Fabricating superhydrophobic lotus-leaf-like surfaces through soft-lithographic imprinting. *Macromol. Rapid Commun.* **2006**, *27* (21), 1859.

(22) Lee, S. M.; Kwon, T. H. Mass-producible replication of highly hydrophobic surfaces from plant leaves. *Nanotechnology* **2006**, *17* (13), 3189.

(23) Cao, A. M.; Cao, L. L.; Gao, D. Fabrication of nonaging superhydrophobic surfaces by packing flowerlike hematite particles. *Appl. Phys. Lett.* **2007**, *91* (3), 034102.

(24) Krupenkin, T. N.; Taylor, J. A.; Schneider, T. M.; Yang, S. From rolling ball to complete wetting: The dynamic tuning of liquids on nanostructured surfaces. *Langmuir* **2004**, *20* (10), 3824.

(25) Jiang, W. H.; Wang, G. J.; He, Y. N. et al. Properties of photoresponsive superhydrophobic azobenzene multilayers fabricated by electrostatic self-assembly. *Chem. J. Chin. Univ.* **2005**, *26* (7), 1360.

(26) Makal, U.; Wynne, K. J. Water induced hydrophobic surface. *Langmuir* **2005**, *21* (9), 3742.

(27) Iijima, S. Helical Microtubules of Graphitic Carbon. *Nature* **1991**, *354* (6348), 56.

(28) Lau, K. K. S.; Bico, J.; Teo, K. B. K.; Chhowalla, M.; Amaratunga, G. A. J.; Milne, W. I.; McKinley, G. H.; Gleason, K. K. Superhydrophobic carbon nanotube forests. *Nano Lett.* **2003**, *3* (12), 1701.

(29) Li, S. H.; Li, H. J.; Wang, X. B.; Song, Y. L.; Liu, Y. Q.; Jiang, L.; Zhu, D. Super-hydrophobicity of large-area honeycomb-like aligned carbon nanotubes. *J. Phys. Chem. B* **2002**, *106* (36), 9274.

(30) Neto, C.; Evans, D. R.; Bonaccurso, E.; Butt, H. J.; Craig, V. S. J. Boundary slip in Newtonian liquids: a review of experimental studies. *Rep. Prog. Phys.* **2005**, *68* (12), 2859.

(31) Walther, J. H.; Werder, T.; Jaffe, R. L.; Gonnet, P.; Bergdorf, M.; Zimmerli, U.; Koumoutsakos, P. Water−carbon interactions III: The influence of surface and fluid impurities. *Phys. Chem. Chem. Phys.* **2004**, *6* (8), 1988.

(32) Zhao, N.; Lu, X. Y.; Zhang, X. Y.; Liu, H. Y.; Tan, S. X.; Xu, J. Progress in superhydrophobic surfaces. *Prog. Chem.* **2007**, *19* (6), 860.

(33) Li, X. M.; Reinhoudt, D.; Crego-Calama, M. What do we need for a superhydrophobic surface? A review on the recent progress in the preparation of superhydrophobic surfaces. *Chem. Soc. Rev.* **2007**, *36* (8), 1350.

(34) Baudry, J.; Charlaix, E.; Tonck, A.; Mazuyer, D. Experimental evidence for a large slip effect at a nonwetting fluid−solid interface. *Langmuir* **2001**, *17* (17), 5232.

(35) Tretheway, D. C.; Meinhart, C. D. Apparent fluid slip at hydrophobic microchannel walls. *Phys. Fluids* **2002**, *14* (3), L9.

(36) Choi, C. H.; Westin, K. J. A.; Breuer, K. S. Apparent slip flows in hydrophilic and hydrophobic microchannels. *Phys. Fluids* **2003**, *15* (10), 2897.

(37) Cassie, A. B. D.; Baxter, S. Wettability of porous surfaces. *Trans. Faraday Soc.* **1944**, *40*, 0546.

(38) Wenzel, R. N. Resistance of solid surfaces to wetting by water. *Ind. Eng. Chem* **1936**, *28*, 988.

(39) Porcheron, F.; Monson, P. A. Mean-field theory of liquid droplets on roughened solid surfaces: Application to superhydrophobicity. *Langmuir* **2006**, *22* (4), 1595.

(40) Yoshimitsu, Z.; Nakajima, A.; Watanabe, T.; Hashimoto, K. Effects of surface structure on the hydrophobicity and sliding behavior of water droplets. *Langmuir* **2002**, *18* (15), 5818.

(41) Joseph, P.; Cottin-Bizonne, C.; Benoît, J. M.; Ybert, C.; Journet, C.; Tabeling, P,; Bocquet, L. Slippage of water past superhydrophobic carbon nanotube forests in microchannels. *Phys. Rev. Lett.* **2006**, *97* (15), 156104.

(42) Sbragaglia, M.; Prosperetti, A. A note on the effective slip properties for microchannel flows with ultrahydrophobic surfaces. *Phys. Fluids* **2007**, *19* (4), 043603.

(43) Ishida, N.; Inoue, T.; Miyahara, M.; Higashitani, K. Nano bubbles on a hydrophobic surface in water observed by tapping-mode atomic force microscopy. *Langmuir* **2000**, *16* (16), 6377.

(44) Tyrrell, J. W. G.; Attard, P. Images of nanobubbles on hydrophobic surfaces and their interactions. *Phys. Rev. Lett.* **2001**, *8717* (17), 176104.

(45) Steitz, R.; Gutberlet, T.; Hauss, T.; Klösgen, B.; Krastev, R.; Schemmel, S.; Simonsen, A. C.; Findenegg, G. H. Nanobubbles and their precursor layer at the interface of water against a hydrophobic substrate. *Langmuir* **2003**, *19* (6), 2409.

(46) Degennes, P. G. Wetting—Statics and Dynamics. *Rev. Mod. Phys.* **1985**, *57* (3), 827.

(47) Adamson, A. W.; Gast, A. P. *Physical Chemistry of Surfaces*, 6th Edition; Wiley: New York, 1997.

(48) Voronov, R. S. Slip Boundary Flow on Nanoscale Superhydrophobic Interfaces: A Molecular Dynamics Study—Slip Length as a Function of Wetting Properties, M.S. Thesis, University of Oklahoma, Norman, OK, 2006.

(49) Young, T. An Essay on the Cohesion of Fluids. *Philos. Trans. R. Soc. London* **1805**, *95*, 65.

(50) Wang, J. Y; Betelu, S; Law, B. M. Line tension approaching a first-order wetting transition: Experimental results from contact angle measurements. *Phys. Rev. E* **2001**, *63* (3), 031601.

(51) Tadros, E. M.; Hu, P.; Adamson, A. W. Adsorption and Contact Angle Studies. 1. Water on Smooth Carbon, Linear Polyethylene, and Stearic Acid-Coated Copper. *J. Colloid Interface Sci.* **1974**, *49* (2), 184.

(52) Extrand, W. C.; Kumagai, Y. Contact angles and hysteresis on soft surfaces. *J. Colloid Interface Sci.* **1996**, *184* (1), 191.

(53) Extrand C. W; Kumagai Y. Wetting and contact angle hysteresis on soft polymer surfaces. *Abstr. Pap. Am. Chem. Soc.* **1996**, 212, 122-COLL.

(54) White, L. R. The contact angle on an elastic substrate. 1. The role of disjoining pressure in the surface mechanics. *J. Colloid Interface Sci.* **2003**, *258* (1), 82.

(55) Eggers, J.; Stone, H. A. Characteristic lengths at moving contact lines for a perfectly wetting fluid: the influence of speed on the dynamic contact angle. *J. Fluid Mech.* **2004**, *505*, 309.

(56) Extrand, C. W. A thermodynamic model for contact angle hysteresis. *J. Colloid Interface Sci.* **1998**, *207* (1), 11.

(57) Extrand, C. W.; Kumagai, Y. An experimental study of contact angle hysteresis. *J. Colloid Interface Sci.* **1997**, *191* (2), 378.

(58) Vega, M. J.; Gouttiere, C.; Seveno, D.; Blake, T. D.; Voue, M.; De Coninck, J. Experimental investigation of the link between static and dynamic wetting by forced wetting of nylon filament. *Langmuir* **2007**, *23* (21), 10628.

(59) Wilson, M. C.; Summers, J. L.; Shikhmurzaev, Y. D.; Clarke, A.; Blake, T. D. Nonlocal hydrodynamic influence on the dynamic contact angle: Slip models versus experiment. *Phys. Rev. E* **2006**, *73* (4), 041606.

(60) Marshall, J. S.; Wang, S. Contact-line fingering and rivulet formation in the presence of surface contamination. *Comput. Fluids* **2005**, *34* (6), 664.

(61) Blake, T. D.; Shikhmurzaev, Y. D. Dynamic wetting by liquids of different viscosity. *J. Colloid Interface Sci.* **2002**, *253* (1), 196.

(62) Lukyanov, A. V.; Shikhmurzaev, Y. D. Effect of flow field and geometry on the dynamic contact angle. *Phys. Rev. E* **2007**, *75* (5), 051604.

(63) Semal, S.; Blake, T. D.; Geskin, V.; de Ruijter, M. J.; Castelein, G.; De Coninck, J. Influence of surface roughness on wetting dynamics. *Langmuir* **1999**, *15* (25), 8765.

(64) Bertrand, E.; Blake, T. D.; Ledauphin, V.; Ogonowski, G.; De Coninck, J. Dynamics of dewetting at the nanoscale using molecular dynamics. *Langmuir* **2007**, *23* (7), 3774.

(65) Eggers, J. Hydrodynamic theory of forced dewetting. *Phys. Rev. Lett.* **2004**, *93* (9), 094502.

(66) Koplik, J.; Banavar, J. R. Molecular simulations of dewetting. *Phys. Rev. Lett.* **2000**, *84* (19), 4401.

(67) Koplik, J; Banavar, J. R. Slip, immiscibility, and boundary conditions at the liquid−liquid interface. *Phys. Rev. Lett.* **2006**, *96* (4), 044505.

(68) Taylor, G. I. Stability of a viscous liquid contained between two rotating cylinders. *Proc. R. Soc. London, Ser. A* **1923**, *102* (718), 541.

(69) Thompson, A. P.; Troian, S. M. A general boundary condition for liquid flow at solid surfaces. *Nature* **1997**, *389* (6649), 360.

(70) Granick, S.; Zhu, Y. X.; Lee, H. Slippery questions about complex fluids flowing past solids. *Nat. Mater.* **2003**, *2* (4), 221.

(71) Koplik, J.; Banavar, J. R.; Willemsen, J. F. Molecular-Dynamics of Fluid-Flow at Solid-Surfaces. *Phys. Fluids, A* **1989**, *1* (5), 781.

(72) Lauga, E.; Stone, H. A. Effective slip in pressure-driven Stokes flow. *J. Fluid Mech.* **2003**, *489*, 55.

(73) Navier, C. L. M. H. *Memoire sur les lois du mouvement des fluids*. Memoires de l'Academie des Sciences de l'Institut de France: 1827; Vol. 6, pp 389−440.

(74) Voronov, R. S.; Papavassiliou, D. V.; Lee, L. L. Boundary slip and wetting properties of interfaces: Correlation of the contact angle with the slip length. *J. Chem. Phys.* **2006**, *124* (20), 204701.

(75) Vinogradova, O. I. Drainage of a Thin Liquid-Film Confined Between Hydrophobic Surfaces. *Langmuir* **1995**, *11* (6), 2213.

(76) Vinogradova, O. I. Implications of hydrophobic slippage for the dynamic measurements of hydrophobic forces. *Langmuir* **1998**, *14* (10), 2827.

(77) Denn, M. M. Extrusion instabilities and wall slip. *Annu. Rev. Fluid Mech.* **2001**, *33*, 265.

(78) Galea, T. M.; Attard, P. Molecular dynamics study of the effect of atomic roughness on the slip length at the fluid-solid boundary during shear flow. *Langmuir* **2004**, *20* (8), 3477.

(79) Zhu, Y. X.; Granick, S. No-slip boundary condition switches to partial slip when fluid contains surfactant. *Langmuir* **2002**, *18* (26), 10058.

(80) Priezjev, N. V.; Troian, S. M. Influence of periodic wall roughness on the slip behaviour at liquid/solid interfaces: molecular-scale simulations versus continuum predictions. *J. Fluid Mech.* **2006**, *554*, 25.

(81) Lauga, E.; Brenner M.; Stone H. Microfluidics: The No-Slip Boundary Condition. In *Springer Handbook of Experimental Fluid Mechanics*; Tropea, C., Foss, J. F., Yarin, A. L., Eds.; Springer−Berlin: Heidelberg, Berlin, Germany, 2007.

(82) Gogte, S.; Vorobieff, P.; Truesdell, R.; Mammoli, A.; van Swol, F.; Shah, P.; Brinker, C. J. Effective slip on textured superhydrophobic surfaces. *Phys. Fluids* **2005**, *17* (5), 051701.

(83) Watanabe, K.; Yanuar Udagawa, H. Drag reduction of Newtonian fluid in a circular pipe with a highly water-repellent wall. *J. Fluid Mech.* **1999**, *381*, 225.

(84) Ellis, J. S.; McHale, G.; Hayward, G. L.; Thompson, M. Contact angle-based predictive model for slip at the solid−liquid interface of a transverse-shear mode acoustic wave device. *J. Appl. Phys.* **2003**, *94* (9), 6201.

(85) Rosen M. J. *Surfactants and Interfacial Phenomena*, 3rd Edition; Wiley−Interscience: Hoboken, NJ, 2004.

(86) Sinha, S. Molecular Dynamics Simulation of Interfacial Tension and Contact Angle of Lennard-Jones Fluid, Ph.D. Dissertation, University of California at Los Angeles, Los Angeles, CA, 2004.

(87) Saville, G. Computer-Simulation of Liquid−Solid−Vapor Contact-Angle. *J. Chem. Soc., Faraday Trans. II* **1977**, *73*, 1122.

(88) Nijmeijer, M. J. P.; Bakker, A. F.; Bruin, C.; Sikkenk, J. H. A Molecular-Dynamics Simulation of the Lennard-Jones Liquid Vapor Interface. *J. Chem. Phys.* **1988**, *89* (6), 3789.

(89) Nijmeijer, M. J. P.; Bruin, C.; Bakker, A. F.; Vanleeuwen, J. M. J. A Visual Measurement of Contact Angles in a Molecular-Dynamics Simulation. *Physica A* **1989**, *160* (2), 166.

(90) Nijmeijer, M. J. P.; Bruin, C.; Bakker, A. F.; Vanleeuwen, J. M. J. Wetting and Drying of an Inert Wall by a Fluid in a Molecular-Dynamics Simulation. *Phys. Rev. A* **1990**, *42* (10), 6052.

(91) Schneemilch, M.; Quirke, N. The interaction of fluids with nanomaterials: Contact angles at nanopatterned interfaces. *Mol. Simul.* **2003**, *29* (10−11), 685.

(92) Schneemilch, M.; Quirke, N.; Henderson, J. R. Wetting of nanopatterned surfaces: The striped surface. *J. Chem. Phys.* **2003**, *118* (2), 816.

(93) Schneemilch, M.; Quirke, N.; Henderson, J. R. Wetting of nanopatterned surfaces: The hexagonal disk surface. *J. Chem. Phys.* **2004**, *120* (6), 2901.

(94) Supple, S.; Quirke, N. Molecular dynamics of transient oil flows in nanopores I: Imbibition speeds for single wall carbon nanotubes. *J. Chem. Phys.* **2004**, *121* (17), 8571.

(95) Sikkenk, J. H.; Indekeu, J. O.; Vanleeuwen, J. M. J.; Vossnack, E. O. Molecular-Dynamics Simulation of Wetting and Drying at Solid−Fluid Interfaces. *Phys. Rev. Lett.* **1987**, *59* (1), 98.

(96) Thompson, P. A.; Robbins, M. O. Simulations of Contact-Line Motion - Slip and the Dynamic Contact-Angle. *Phys. Rev. Lett.* **1989**, *63* (7), 766.

(97) Guillot, B. A reappraisal of what we have learnt during three decades of computer simulations on water. *J. Mol. Liq.* **2002**, *101* (1−3), 219.

(98) Berendsen, H. J. C.; Grigera, J. R.; Straatsma, T. P. The Missing Term in Effective Pair Potentials. *J. Phys. Chem.* **1987**, *91* (24), 6269.

(99) Jorgensen, W. L.; Chandrasekhar, J.; Madura, J. D.; Impey, R. W.; Klein, M. L. Comparison of Simple Potential Functions for Simulating Liquid Water. *J. Chem. Phys.* **1983**, *79* (2), 926.

(100) Kiyohara, K.; Gubbins, K. E.; Panagiotopoulos, A. Z. Phase coexistence properties of polarizable water models. *Mol. Phys.* **1998**, *94* (5), 803.

(101) MacKerell, A. D.; Bashford, D.; Bellott, M.; Dunbrack, R. L., Jr.; Evanseck, J. D.; Field, M. J.; Fischer, S.; Gao, J.; Guo, H.; Ha, S.; Joseph-McCarthy, D.; Kuchnir, L.; Kuczera, K.; Lau, F. T. K.; Mattos, C.; Michnick, S.; Ngo, T.; Nguyen, D. T.; Prodhom, B.; Reiher, W. E., III.; Roux, B.; Schlenkrich, M.; Smith, J. C.; Stote, R.; Straub, J.; Watanabe, M.; Wiórkiewicz-Kuczera, J.; Yin, D.; Karplus, M. All-atom empirical potential for molecular modeling and dynamics studies of proteins. *J. Phys. Chem. B* **1998**, *102* (18), 3586.

(102) Hautman, J.; Klein, M. L. Microscopic Wetting Phenomena. *Phys. Rev. Lett.* **1991**, *67* (13), 1763.

(103) Mar, W.; Klein, M. L. A Molecular-Dynamics Study of *N*-Hexadecane Droplets on a Hydrophobic Surface. *J. Phys.: Condens. Matter* **1994**, *6*, A381.

(104) Gordillo, M. C.; Nagy, G.; Martí, J. Structure of water nanoconfined between hydrophobic surfaces. *J. Chem. Phys.* **2005**, *123* (5), 054707.

(105) Striolo, A.; Chialvo, A. A.; Gubbins, K. E.; Cummings, P. T. Water in carbon nanotubes: Adsorption isotherms and thermodynamic properties from molecular simulation. *J. Chem. Phys.* **2005**, *122* (23), 234712.

(106) Striolo, A.; Gubbins, K. E.; Gruszkiewicz, M. S.; Cole, D. R.; Simonson, J. M.; Chialvo, A. A. Effect of temperature on the adsorption of water in porous carbons. *Langmuir* **2005**, *21* (21), 9457.

(107) Lundgren, M.; Allan, N. L.; Cosgrove, T.; George, N. Molecular dynamics study of wetting of a pillar surface. *Langmuir* **2003**, *19* (17), 7127.

(108) Lundgren, M.; Allan, N. L.; Cosgrove, T. Wetting of water and water/ethanol droplets on a non-polar surface: A molecular dynamics study. *Langmuir* **2002**, *18* (26), 10462.

(109) Moulin, F.; Devel, M.; Picaud, S. Molecular dynamics simulations of polarizable nanotubes interacting with water. *Phys. Rev. B* **2005**, *71* (16), 165401.

(110) Liu, Y. C.; Wang, Q. Transport behavior of water confined in carbon nanotubes. *Phys. Rev. B* **2005**, *72* (8), 085420.

(111) Pertsin, A.; Grunze, M. Water−graphite interaction and behavior of water near the graphite surface. *J. Phys. Chem. B* **2004**, *108* (4), 1357.

(112) Koumoutsakos, P.; Walther, J.; Werder, T.; Zimmerli, U.; Jaffe, R. Water−carbon nanotube interactions: Potential energy calibration for molecular dynamics simulations using experiments and quantum system calculations. *Abstr. Pap. Am. Chem. Soc.* **2003**, *225*, U705.

(113) Jaffe, R. L.; Gonnet, P.; Werder, T.; Walther, J. H.; Koumoutsakos, P. Water−carbon interactions−2: Calibration of potentials using contact angle data for different interaction models. *Mol. Simul.* **2004**, *30* (4), 205.

(114) Janecek, J.; Netz, R. R. Interfacial water at hydrophobic and hydrophilic surfaces: Depletion versus adsorption. *Langmuir* **2007**, *23* (16), 8417.

(115) Cao, B. Y.; Chen, M.; Guo, Z. Y. Liquid flow in surface-nanostructured channels studied by molecular dynamics simulation. *Phys. Rev. E* **2006**, *74* (6), 066311.

(116) Cieplak, M.; Koplik, J.; Banavar, J. R. Nanoscale fluid flows in the vicinity of patterned surfaces. *Phys. Rev. Lett.* **2006**, *96* (11), 114502.

(117) Honig, C. D.; Ducker, W. A. No-slip hydrodynamic boundary condition for hydrophilic particles. *Phys. Rev. Lett.* **2007**, *98* (2), 028305.

(118) Denn, M. M. Fifty years of non-Newtonian fluid dynamics. *AIChE J.* **2004**, *50* (10), 2335.

(119) Li, D.; Di, Q. F.; Li, J. Y.; Qian, Y. H.; Fang, H. P. Large slip length over a nanopatterned surface. *Chin. Phys. Lett.* **2007**, *24* (4), 1021.

(120) Restagno, F.; Crassous, J.; Charlaix, E.; Cottin-Bizonne, C.; Monchanin, M. A new surface forces apparatus for nanorheology. *Rev. Sci. Instrum.* **2002**, *73* (6), 2292.

(121) Claesson, P. M.; Ederth, T.; Bergeron, V.; Rutland, M. W. Techniques for measuring surface forces. *Adv. Colloid Interface Sci.* **1996**, *67*, 119.

(122) Butt, H. J.; Berger, R.; Bonaccurso, E.; Chen, Y.; Wang, J. Impact of atomic force microscopy on interface and colloid science. *Adv. Colloid Interface Sci.* **2007**, *133* (2), 91.

(123) Giessibl, F. J. Advances in atomic force microscopy. *Rev. Mod. Phys.* **2003**, *75* (3), 949.

(124) Craig, V. S.; Neto, C.; Williams, D. R. Shear-dependent boundary slip in an aqueous Newtonian liquid. *Phys. Rev. Lett.* **2001**, 8705 (5), 054504.

(125) Lauga, E. Apparent slip due to the motion of suspended particles in flow of electrolyte solutions. *Langmuir* **2004**, *20* (20), 8924.

(126) Jin, S.; Huang, P.; Park, J.; Yoo, J. Y.; Breuer, K. S. Near-surface velocimetry using evanescent wave illumination. *Exp. Fluid* **2004**, *37* (6), 825.

(127) Pit, R.; Hervet, H.; Leger, L. Friction and slip of a simple liquid at a solid surface. *Tribol. Lett.* **1999**, *7* (2−3), 147.

(128) Schmatko, T.; Hervet, H.; Leger, L. Friction and slip at simple fluid−solid interfaces: The roles of the molecular shape and the solid−liquid interaction. *Phys. Rev. Lett.* **2005**, *94* (24), 244501.

(129) Huang, P.; Guasto, J. S.; Breuer, K. S. Direct measurement of slip velocities using three-dimensional total internal reflection velocimetry. *J. Fluid Mech.* **2006**, *566*, 447.

(130) Huang, P.; Breuer, K. S. Direct measurement of slip length in electrolyte solutions. *Phys. Fluids* **2007**, *19* (2), 028104.

(131) Zhu, Y. X.; Granick, S. Rate-dependent slip of Newtonian liquid at smooth surfaces. *Phys. Rev. Lett.* **2001**, *8709* (9), 096105.

(132) (a) Majumder, M.; Chopra, N.; Andrews, R.; Hinds, B. J. Nanoscale hydrodynamics: Enhanced flow in carbon nanotubes. *Nature* **2005**, *438* (7064), 44. (b) Majumder, M.; Chopra, N.; Andrews, R.; Hinds, B. J. Erratum. *Nature* **2005**, *438* (7070), 930.

(133) Cottin-Bizonne, C.; Cross, B.; Steinberger, A.; Charlaix, E. Boundary slip on smooth hydrophobic surfaces: Intrinsic effects and possible artifacts. *Phys. Rev. Lett.* **2005**, *94* (5), 056102.

(134) Choi, C.-H.; Kim, C.-J. Large slip of aqueous liquid flow over a nanoengineered superhydrophobic surface. *Phys. Rev. Lett.* **2006**, *96* (6), 066001.

(135) Neto, C.; Craig, V. S. J.; Williams, D. R. M. Evidence of shear-dependent boundary slip in newtonian liquids. *Eur. Phys J., E* **2003**, *12*, 71.

(136) Truesdell, R.; Mammoli, A.; Vorobieff, P.; van Swol, F.; Brinker, C. J. Drag reduction on a patterned superhydrophobic surface. *Phys. Rev. Lett.* **2006**, *97* (4), 044504.

(137) Cross, B.; Steinberger, A.; Cottin-Bizonne, C.; Rieu, J. P.; Charlaix, E. Boundary flow of water on supported phospholipid films. *Europhys. Lett.* **2006**, *73* (3), 390.

(138) Barrat, J. L.; Bocquet, L. Influence of wetting properties on hydrodynamic boundary conditions at a fluid/solid interface. *Faraday Discuss.* **1999**, (112), 119.

(139) Barrat, J. L.; Bocquet, L. Large slip effect at a nonwetting fluid−solid interface. *Phys. Rev. Lett.* **1999**, *82* (23), 4671.

(140) Zhu, L. D.; Tretheway, D.; Petzold, L.; Meinhart, C. Simulation of fluid slip at 3D hydrophobic microchannel walls by the lattice Boltzmann method. *J. Comput. Phys.* **2005**, *202* (1), 181.

(141) Benzi, R.; Biferale, L.; Sbragaglia, M.; Succi, S.; Toschi, F. Mesoscopic modelling of local phase transitions and apparent-slip phenomena in microflows. *Math. Comput. Simul.* **2006**, *72* (2−6), 84.

(142) Sbragaglia, M.; Succi, S. Analytical calculation of slip flow in lattice Boltzmann models with kinetic boundary conditions. *Phys. Fluids* **2005**, *17* (9), 093602.

(143) Lennard-Jones, J. E. Cohesion. *Proc. Phys. Soc.* **1931**, *43*, 461.

(144) Koplik, J.; Banavar, J. R.; Willemsen, J. F. Molecular Dynamics of Fluid Flow at Solid Surfaces. *Phys. Fluids, A* **1989**, *1* (5), 781.

(145) Thompson, P. A.; Robbins, M. O. Shear-Flow Near Solids−Epitaxial Order and Flow Boundary-Conditions. *Phys. Rev. A* **1990**, *41* (12), 6830.

(146) Morris, D. L.; Hannon, L.; Garcia, A. L. Slip Length in a Dilute Gas. *Phys. Rev. A* **1992**, *46* (8), 5279.

(147) Yang, S. C. Effects of surface roughness and interface wettability on nanoscale flow in a nanochannel. *Microfluid. Nanofluid.* **2006**, *2* (6), 501.

(148) Jabbarzadeh, A.; Atkinson, J. D.; Tanner, R. I. Effect of the wall roughness on slip and rheological properties of hexadecane in molecular dynamics simulation of Couette shear flow between two sinusoidal walls. *Phys. Rev. E* **2000**, *61* (1), 690.

(149) Cieplak, M.; Koplik, J.; Banavar, J. R. Boundary conditions at a fluid−solid interface. *Phys. Rev. Lett.* **2001**, *86* (5), 803.

(150) Sokhan, V. P.; Nicholson, D.; Quirke, N. Fluid flow in nanopores: An examination of hydrodynamic boundary conditions. *J. Chem. Phys.* **2001**, *115* (8), 3878.

(151) Sokhan, V. P.; Nicholson, D.; Quirke, N. Fluid flow in nanopores: Accurate boundary conditions for carbon nanotubes. *J. Chem. Phys.* **2002**, *117* (18), 8531.

(152) Walther, J. H.; Werder, T.; Jaffe, R. L.; Koumoutsakos, P. Hydrodynamic properties of carbon nanotubes. *Phys. Rev. E* **2004**, *69* (6), 062201.

(153) Koplik, J.; Banavar, J. R.; Willemsen, J. F. Molecular Dynamics of Fluid Flow at Solid Surfaces. *Phys. Fluids, A* **1989**, *1* (5), 781.

(154) Brenner, D. W. Empirical Potential for Hydrocarbons for Use in Simulating the Chemical Vapor-Deposition of Diamond Films. *Phys. Rev. B* **1990**, *42* (15), 9458.

(155) Priezjev, N. V.; Darhuber, A. A.; Troian, S. M. Slip behavior in liquid films on surfaces of patterned wettability: Comparison between continuum and molecular dynamics simulations. *Phys. Rev. E* **2005**, *71* (4), 041608.

(156) Yang, S. C.; Fang, L. B. Effect of surface roughness on slip flows in hydrophobic and hydrophilic microchannels by molecular dynamics simulation. *Mol. Simul.* **2005**, *31* (14−15), 971.

(157) Blake, T. D. Slip Between a Liquid and a Solid - Tolstoi, D. M. (1952) Theory Reconsidered. *Colloids Surf.* **1990**, *47*, 135.

(158) Benzi, R.; Biferale, L.; Sbragaglia, M.; Succi, S.; Toschi, F. Mesoscopic modeling of a two-phase flow in the presence of boundaries: The contact angle. *Phys. Rev. E* **2006**, *74* (2), 021509.

(159) Voronov, R. S.; Papavassiliou, D. V.; Lee, L. L. Slip length and contact angle over hydrophobic surfaces. *Chem. Phys. Lett.* **2007**, *441*, 273.

(160) Plimpton, S. Fast Parallel Algorithms for Short-Range Molecular-Dynamics. *J. Comput. Phys.* **1995**, *117* (1), 1. (Also available via the Internet a tthe following URL: http://www.cs.sandia.gov/~sjplimp/lammps.html)

(161) Graphite v3.0 Web-based extended graphite lattice generator, 2005. (Computer program.)

(162) Heinbuch, U.; Fischer, J. Liquid Flow in Pores−Slip, No-Slip, or Multilayer Sticking. *Phys. Rev. A* **1989**, *40* (2), 1144.

(163) Israelachvili, J. N. Measurement of the Viscosity of Liquids in Very Thin-Films. *J. Colloid Interface Sci.* **1986**, *110* (1), 263.

(164) Israelachvili, J. N. Measurements of the Viscosity of Thin Fluid Films Between 2 Surfaces with and without Adsorbed Polymers. *Colloid. Polym. Sci.* **1986**, *264* (12), 1060.

(165) Ackerson, B. J.; Pusey, P. N. Shear-Induced Order in Suspensions of Hard-Spheres. *Phys. Rev. Lett.* **1988**, *61* (8), 1033.

(166) Bocquet, L.; Barrat, J. L. Hydrodynamic Boundary-Conditions, Correlation-Functions, and Kubo Relations for Confined Fluids. *Phys. Rev. E* **1994**, *49* (4), 3079.

(167) Matsushita, K.; Matsukawa, H.; Sasaki, N. Atomic scale friction between clean graphite surfaces. *Solid State Commun.* **2005**, *136* (1), 51.

(168) Extrand, C. W.; Moon, S. I.; Hall, P.; Schmidt, D. Superwetting of structured surfaces. *Langmuir* **2007**, *23* (17), 8882.

(169) Lundgren, M.; Allan, N. L.; Cosgrove, T. Modeling of wetting: A study of nanowetting at rough and heterogeneous surfaces. *Langmuir* **2007**, *23* (3), 1187.

(170) Extrand, C. W. Contact angles and hysteresis on surfaces with chemically heterogeneous islands. *Langmuir* **2003**, *19* (9), 3793.

(171) Philip, J. R. Flows Satisfying Mixed No-Slip and No-Shear Conditions. *Z. Angew. Math. Phys.* **1972**, *23* (3), 353.

(172) Philip, J. R. Integral Properties of Flows Satisfying Mixed No-Slip and No-Shear Conditions. *Z. Angew. Math. Phys.* **1972**, *23* (6), 960.

(173) Cottin-Bizonne, C.; Barrat, J. L.; Bocquet, L.; Charlaix, E. Low-friction flows of liquid at nanopatterned interfaces. *Nat. Mater.* **2003**, *2* (4), 237.

(174) Peraltafabi, R.; Zwanzig, R. On the Slipping Boundary-Condition for Low-Density Gas-Flow. *J. Chem. Phys.* **1983**, *78* (5), 2525.

(175) Lichter, S.; Roxin, A.; Mandre, S. Mechanisms for liquid slip at solid surfaces. *Phys. Rev. Lett.* **2004**, *93* (8), 086001.

(176) Richards, S. No-Slip Boundary-Condition. *J. Fluid Mech.* **1973**, *59* (AUG7), 707.

(177) Zwanzig, R. Rotational Friction Coefficients of a Bumpy Cylinder with Slipping and Sticking Boundary-Conditions. *J. Chem. Phys.* **1978**, *68* (9), 4325.

(178) Tretheway, D. C.; Meinhart, C. D. A generating mechanism for apparent fluid slip in hydrophobic microchannels. *Phys. Fluids* **2004**, *16* (5), 1509.

(179) Buckingham, E. On physically similar systems, illustrations of the use of dimensional equations. *Phys. Rev.* **1914**, *4* (4), 345.

(180) Sprittles, J. E.; Shikhmurzaev, Y. D. Viscous flow over a chemically patterned surface. *Phys. Rev. E* **2007**, *76* (2), 021602.

(181) Andrienko, D.; Dunweg, B.; Vinogradova, O. I. Boundary slip as a result of a prewetting transition. *J. Chem. Phys.* **2003**, *119* (24), 13106.

(182) Li, Y. X.; Xu, J. L. A new criterion number for the boundary conditions at the solid/liquid interface in nanoscale. *Nanoscale Microscale Thermophys. Eng.* **2006**, *10* (2), 109.

(183) Sullivan, D. E. Surface-Tension and Contact-Angle of a Liquid-Solid Interface. *J. Chem. Phys.* **1981**, *74* (4), 2604.

(184) Cuadros, F.; Cachadina, I.; Ahumada, W. Determination of Lennard-Jones interaction parameters using a new procedure. *Mol. Eng.* **1996**, *6* (3), 319.

Received for review September 26, 2007
Revised manuscript received January 10, 2008
Accepted January 14, 2008

IE0712941